Accepted Manuscript

Survey on deep learning for radiotherapy

Philippe Meyer, Vincent Noblet, Christophe Mazzara, Alex Lallement

PII: S0010-4825(18)30131-8

DOI: 10.1016/j.compbiomed.2018.05.018

Reference: CBM 2969

To appear in: *Computers in Biology and Medicine*

Received Date: 3 March 2018

Revised Date: 15 May 2018

Accepted Date: 15 May 2018

Please cite this article as: P. Meyer, V. Noblet, C. Mazzara, A. Lallement, Survey on deep learning for radiotherapy, *Computers in Biology and Medicine* (2018), doi: 10.1016/j.compbiomed.2018.05.018.

SURVEY ON DEEP LEARNING FOR RADIOTHERAPY

Philippe Meyer[a], Vincent Noblet[b], Christophe Mazzara[a], Alex Lallement[b]

[a]Department of Medical Physics, Paul Strauss Center, Strasbourg, France

[b]ICube-UMR 7357, Strasbourg, France

Corresponding author : Philippe MEYER, PhD, 3 rue de la porte de l'hôpital, 67000 Strasbourg, France. Tel : 33388258544 ; E-mail : pmeyer@strasbourg.unicancer.fr

Conflict of interest: none declared.

Abstract

More than 50% of cancer patients are treated with radiotherapy, either exclusively or in combination with other methods. The planning and delivery of radiotherapy treatment is a complex process, but can now be greatly facilitated by artificial intelligence technology. Deep learning is the fastest-growing field in artificial intelligence and has been successfully used in recent years in many domains, including medicine.

In this article, we first explain the concept of deep learning, addressing it in the broader context of machine learning. The most common network architectures are presented, with a more specific focus on convolutional neural networks. We then present a review of the published works on deep learning methods that can be applied to radiotherapy, which are classified into seven categories related to the patient workflow, and can provide some insights of potential future applications. We have attempted to make this paper accessible to both radiotherapy and deep learning communities, and hope that it will inspire new collaborations between these two communities to develop dedicated radiotherapy applications.

Keywords:

Radiotherapy

Deep-learning

Convolutional Networks

1. Introduction

Patient workflow in radiotherapy is one of the most complex workflows. There are many steps involved: choice of the radiotherapy treatment scheme; image acquisition of the patient in treatment position; segmentation of the target volumes and organs-at-risk (OAR) using multimodal imaging; treatment planning; delivery of treatment including monitoring of patient positioning, movements, and delivered dose; and finally, post-treatment follow-up.

To facilitate and improve the efficiency of this workflow, artificial intelligence (AI) systems have been proposed for automatic organ segmentation, error prevention, or treatment planning [1,2]. However, these systems are still seldom used in clinical routines. For instance, manual delineation of target volumes and OAR is still the standard routine for most clinical centers, even though it is time consuming and prone to intra- and inter-observer variations [3]. One issue is the limited performance of current commercial software. In radiotherapy, toxic and fatal doses are sometimes delivered at 1 or 2 mm from risk organs; therefore, it is vital that segmentation is extremely accurate (see Fig. 1). However, current automatic segmentation software cannot achieve the necessary level of accuracy. Consequently, radiation oncologists may lose more time correcting automatically segmented structures than by manually segmenting the structures themselves.

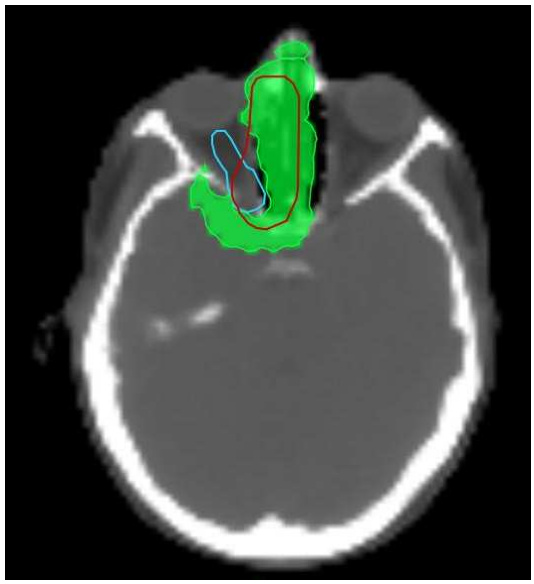

Fig 1. Planned dose distribution for nasopharyngeal cancer treatment. The 54-Gy isodose (in green) should cover the target volume (in red) and must not cover the optic nerve (in blue), because the risk of blindness becomes too high when doses exceeding 54 Gy are used. This case illustrates the extreme accuracy required for the segmentation of organs in radiotherapy.

Deep learning (DL) is a branch of AI and machine learning, which has enjoyed considerable success in recent years in diverse fields including science, business, and government. DL has dramatically supplanted other machine learning methods for applications such as recognition and image processing in computer vision, by achieving human-equivalent performance on some tasks [4–6]. DL techniques also open promising perspectives in AI applied to radiotherapy and may significantly improve the radiotherapy patient workflow in the coming years [7,8]. To illustrate the rapidly

evolving interest aroused by these new techniques in radiotherapy, Fig. 2 shows the number of DL papers published in this field since 2012.

Several reviews about DL in medical imaging have already been published [5,9–11], but none were specifically dedicated to radiotherapy. In this paper, we first explain the basic concepts of machine learning, in Section 2, adapted to radiation oncologists and medical physicists. We then present a simple introduction to DL and to the different network architectures, with a focus on convolutional neural networks (CNNs). In Section 3, we present a brief review of research works in which DL methods are or could potentially be applied to a step of the radiotherapy workflow, trying to make it accessible to non-radiotherapy specialists. We have chosen to classify the reviewed papers into seven categories relevant to the different radiotherapy steps. These categories are as follows: *images used for radiotherapy planning and treatment setup*, *image segmentation, computer-aided detection and diagnosis, image registration, treatment planning, motion management/patient setup during treatment*, and *medical data extraction and outcome prediction in radiotherapy*. Note that a survey mainly dedicated to DL-based medical image segmentation and computer-aided detection tasks has recently been proposed by Litjens et al., who reviewed 306 papers [5]. Other reviews also exist for medical data extraction by DL [12–14]. Therefore, we have not conducted exhaustive reviews for these specific categories but we have selected articles of particular importance in radiotherapy.

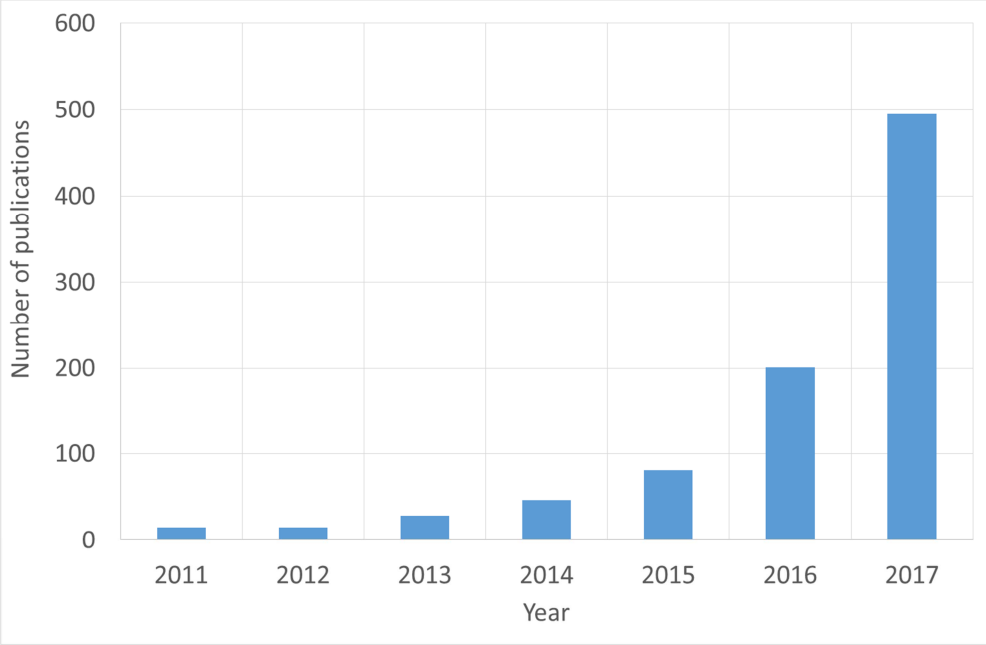

Fig. 2. Number of publications for the search phrases with at least the terms *radiotherapy* or *radiation therapy* or *radiation oncology* and at least the terms *deep learning* or *deep network* or *convolutional network*. Publication statistics are obtained from Google Scholar.

2. What is deep learning?

DL describes a set of computational models composed of multiple layers of data processing, which make it possible to learn by representing these data through several levels of abstraction [4,15–17].

From a large amount of training data, these models discover recurrent structures by automatically refining their internal parameters via a backpropagation algorithm. Each layer of the network transforms the signal nonlinearly in order to increase the selectivity and invariance of the representation. With a sufficient number of layers, the network can generate a hierarchy of representations that will make the model both sensitive to very small details and insensitive to large variations. In recent years, DL has been successfully used to solve real problems in a wide range of applications. However, because the underlying tuned model is composed of millions of parameters, there is still no clear understanding of the inner working mechanisms. Thus, many time-consuming trial-and-errors procedures are required to correctly train the model.

DL approaches are part of the so-called *machine learning*, which is a field of AI. CNN is a special approach to DL, dedicated to image processing (Fig. 3). Machine learning, DL, and CNN are explained respectively in Sections 2.1, 2.2, and 2.3.

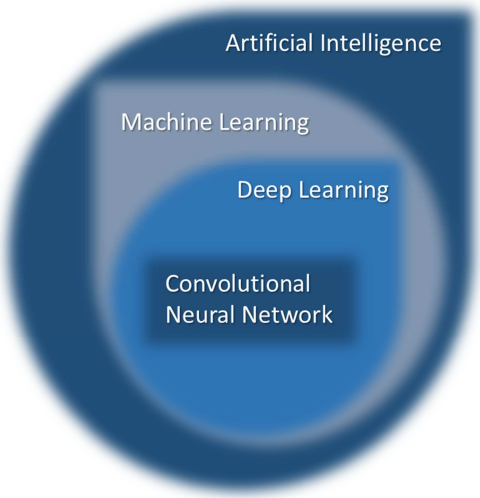

Fig. 3. A possible classification of some artificial intelligence methods.

2.1 Machine learning

The term AI was introduced in 1956 by one of the pioneers of the field, John McCarthy [18,19]. Boden defined AI as a science, whose purpose is to make machines perform tasks that would require human intelligence [20]. If we consider contemporary AI, several authors cited the article *Computing machinery and intelligence* published in 1950 as one of the founding works [21]. Six years later, Newell and Simon proposed the *logic theorist algorithm*, often considered as the first computer program in the field of AI, which opened the way to the many AI methods we currently know [22]. Among these methods, machine learning was proposed for the first time in 1959 by Samuel, who developed an AI program that can play checkers based on partial setting using the experience gained [23].

Considering that designing and programming explicit models for complex tasks with satisfactory performance is sometimes difficult or infeasible, machine learning attempts to make data-driven

decisions by automatically building a model from large-scale training data [24, 25]. The key concept of machine learning is thus to produce accurate predictions on new unseen data after being trained on a finite learning dataset, in other words, to generalize from limited experience.

To concretely define what *learning* means, Mitchell et al. proposed to specify three parameters, namely T, P, and E [26]: "a computer program is said to learn from experience E with respect to some class of tasks T and performance measure P if its performance on tasks in T, as measured by P, improves with experience E." Table 1 provides radiotherapy application examples to illustrate this proposal.

Examples of machine learning scenarios include supervised, unsupervised, reinforcement, and transfer learning [27]. In supervised learning, the algorithm is presented with training inputs and their corresponding desired outputs (i.e., labels); the goal is to learn a rule that maps inputs to outputs. For example, a set of quantitative features extracted from a mammography image can be considered as input and the corresponding expert diagnosis (cancerous versus healthy) as the desired output. The goal is then to automatically categorize new mammograms that have not been evaluated by an expert (i.e., classification) [28]. In unsupervised learning, no referenced outputs are given to the algorithm and the goal is to find a structure in the inputs. As examples, one can imagine distinguishing patients at risk from other patients based on clinical notes extracted from electronic health record (EHR) systems (i.e., clustering) [29], or to learn high-level features from images (i.e., dimensionality reduction) [30]. In reinforcement learning, the algorithm must perform a certain goal through interaction with its dynamic environment. A feedback is used to adjust the learning process in a way to maximize long-term rather than immediate reward trade-offs. Reinforcement learning is thus based on communication and exploration rather than on explicit education. This type of approach can be used, for example, to study different scenarios of tumor growth and radiotherapy [31]. For many medical applications, only a small amount of training data is often available, mostly due to confidentiality reasons or incomplete information. Because the available input data are insufficient to train a network from scratch, transfer learning aims to use a pre-trained network to perform another task that it was not originally intended for. An additional training step is then performed using a small amount of labeled data to fine-tune the network weights [32].

2.2 Deep neural networks

Deep neural networks (DNNs) are forms of machine learning methods. In machine learning, it is often necessary to reduce the complexity of the input data and make relevant patterns more visible for the learning algorithms to function. Indeed, their performance greatly depends on how accurately these features have been identified and extracted. Given that this feature engineering process is based on domain knowledge and is specific to the data type, it is difficult and expensive in terms of time and expertise to apply. In contrast, DNNs independently learn a hierarchical representation of the input data adapted to the task at hand; this eliminates the task of developing new features extractors for every problem. The main drawback is that DNNs require a large amount of input data to be effective. The idea of a computer program that could find itself representing a model from a dataset is not new. Perceptron is one of the first approaches to conceptualize data directly from the environment

[33]. It is inspired by the biology of the brain: an artificial neuron is a mathematical function conceived as a coarse model of a biological neuron (Fig. 4). The principle is to simulate the transfer of information through a neuron: weighted nodes receive the inputs (representing the synapses), sum them to produce an activation (representing the axon), and pass this activation to a nonlinear function called activation or transfer function, in order to generate the output signal. Each neuron acts as an elementary processing unit. The output signal of one unit will feed the other units, organized in layers, and so on, forming an artificial neural network (ANN). When it is composed of several intermediate hidden layers, it is called *multilayer neural networks* or DNNs (Fig. 5). Note that the multilayer perceptron (MLPs) is an intermediate link in the transition from the simple perceptron to the DNN. DNNs are a recent advance in the field that conceptually expands the MLP by adding a significant number of layers (instead of 1 to 3 that the typical MLP has).

Example learning problem	**Task T**	**Performance measure P**	**Training experience E**
Learning checkers	Playing checkers	Percentage of games won against opponents	Learner playing practice games against itself
Handwriting recognition	Recognizing handwritten words	Percentage of words correctly recognized	Handwritten words with given classification
Self-driving car	Driving from Hochfelden to Saint-Claude	Distance traveled before an error (as judged by a human overseer)	Videos, images, and steering commands recorded while observing a human driver
Automatic segmentation of medical images	Segment the prostate on MRI	Percentage of common pixels between automatic and human expert segmentation	MRI database with prostate segmented by human experts
Computer-aided detection on medical images	To detect brain metastases (BM) on MRI	Percentage of false negative or false positive (FP)	MRI database with BM segmented by human experts
Dose calculation on MRI	To generate a pseudo-computed tomography (CT) image from an MRI	Average mean difference of Hounsfield units between the pseudo-CT and a reference CT image	Database with registered MRI and CT images
Image-guided radiotherapy dose reduction	To reduce noise in fluoroscopic kV images	Signal to noise ratio difference between a corrected kV image and the mean of 10 kV images	Database of fluoroscopic kV patient images during radiotherapy treatment
Automatic treatment planning help	To predict planned dose from organ segmentation	Percentage of common pixels between predicted and calculated dose	Database of RT structures and RT dose files
Avoidance of patient collision during radiotherapy treatment	To recognize and classify objects and patient inside the treatment room	Percentage of correctly classified objects	Database of classified objects
Decision-making tool for radiation oncologists	To predict rectal toxicity after cervical cancer radiotherapy	Difference between real and predicted toxicities	Database of radiotherapy treatment plans including RT structures and dose files + medical database with rectal toxicity evaluation

Table 1. Some examples related to machine learning problems. The first 3 lines are taken from [26] and [25]. The other examples (in gray) are taken from published applications of machine learning in radiotherapy, which can be found in Section 3.

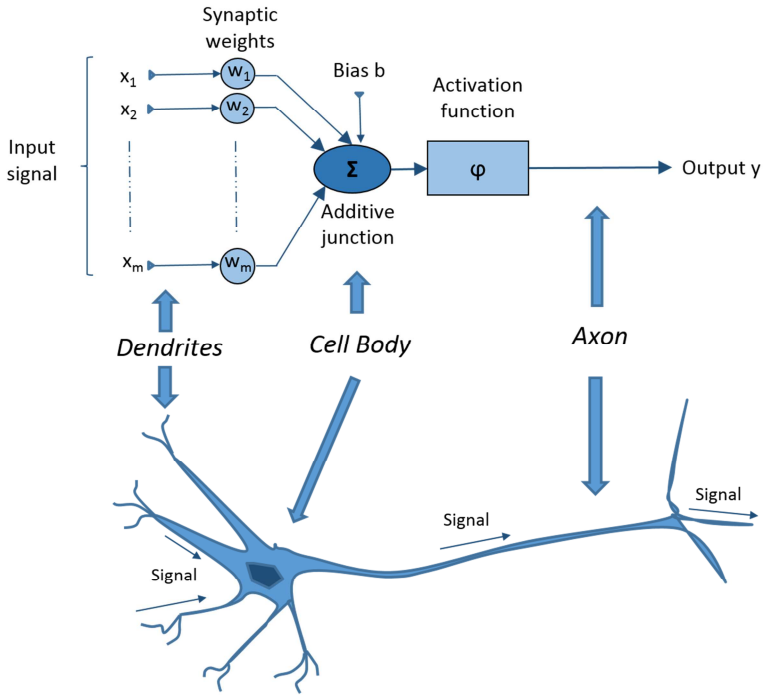

Fig. 4. Analogy between an artificial neuron and a biological neuron. The input signals are represented by x. The bias b and the activation function φ can be parameterized by the user. Weights *w* are adjusted automatically by the network.

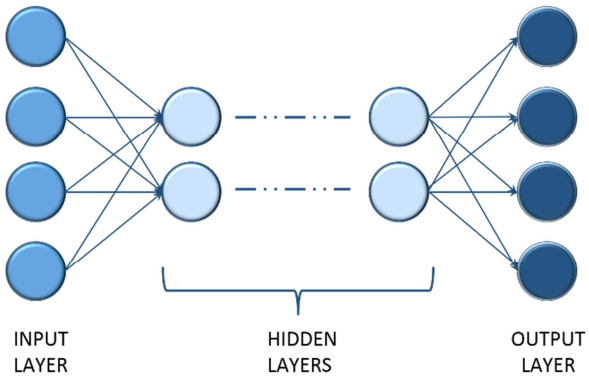

Fig. 5. Schematic illustration of a deep neural network. Neurons not contained in the input or output layer are contained in the hidden layers.

Actually, DL uses a cascade of multiple layers of nonlinear processing units for feature extraction and transformation, with each successive layer using the output from the previous layer as input. The first layer is the input layer that receives the dataset. The last layer is the output layer that delivers the result. In between, layers transforming the signal are called hidden layers. The underlying assumption is that these successive hidden layers correspond to levels of abstraction. Varying the number, size, and composition of each layer can thus provide different amounts of abstraction, and

allows high-level features to be derived from low-level features in order to form a hierarchical representation. The challenge is to find the appropriate level of granularity, given the size and dimension of the available training dataset and the complexity of the task. Note that high-level feature extraction (abstraction), which indeed takes place, creates features that are very difficult for humans to interpret meaningfully and match to metrics of observable procedures.

The training process

It is important to keep in mind that a neural network must be trained in a dedicated phase. Training a neural network consists of learning each neuron's weights (*w* in Fig. 4). In supervised learning, it can be formulated as an error function minimization between the network's output (the prediction) and the desired output (the labels). As this error function is highly nonlinear and non-convex, there is no analytical solution that can minimize it. The usual solution is to update the weights iteratively by means of a backpropagation gradient algorithm [34,35], the most commonly used being the *stochastic gradient descent*. At first, all the weights are randomly initialized. Then the output of the network is computed with respect to the training input. The gradient can be efficiently computed by propagating errors from the output layer back to the input layer by a chain rule. Once the gradient vector is computed for all layers, the weights can be updated. This update process repeats until convergence is reached or a predefined number of iterations have been performed.

The transfer function and the bias are fixed and user-definable. The transfer function is usually defined as monotonically increasing, continuous, differentiable, and bounded. The most popular transfer function is called rectified linear unit (ReLU), which allows fast learning of DNNs (Fig. 6).

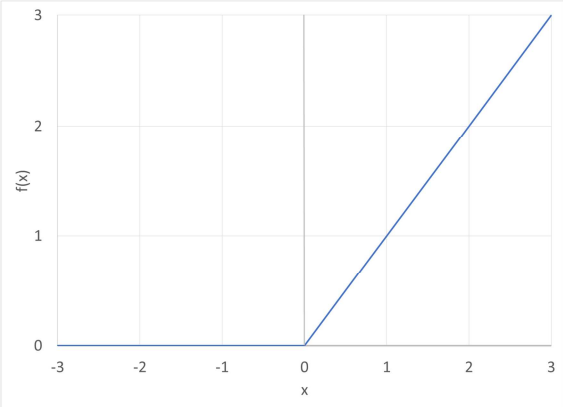

Fig. 6. Rectified linear unit transfer function (ReLU) commonly used in deep neural networks.

Why deep learning now?

Recently qualified as DL, we saw that research on DNNs dates back to the 1950s and actually has a long and rich history [15]. Multilayered networks are not convincing and attracted only a few researchers worldwide for many years [4]. The renewal of interest on DL was catalyzed in 2006 by the grouping of a few researchers by a Canadian institute. Since then, DL has been able to respond to increasingly complex applications, with ever-greater accuracy.

The reasons for this sudden success can be traced in the 2012 ImageNet competition, when a team (the only one to use a DL architecture) was able to halve the rate of misclassification [36]. The

success of the network developed by Krizhevsky et al. is due to its architecture, the power of calculations on graphics processing unit (GPU), and the large amount of training data. The combination of these three factors currently places DL at the forefront of AI approaches. The GPU calculation makes it possible to manage the memory required for the learning and adjustment processes of billions of weights of contemporary networks in an acceptable time. To generalize correctly, it is imperative that the number of training data should be large enough to represent reality. Note that these properly labeled databases are potentially difficult to obtain in the medical field, which can be a hindrance to the deployment of DL methods. The last factor that led to the emergence of DL is the improvement in network architectures, which has recently benefited from numerous developments.

Network architectures commonly used in deep learning

Many DL network architectures have been developed depending on specific applications or learning data. Several classifications are possible, which are detailed in the following references dedicated to medical applications [5,13,14,37]. Ravi et al., specifically provided a classification of the different architectures according to particular applications in the medical field. Here, we briefly describe the architectures most frequently used in radiotherapy applications (Fig. 7).

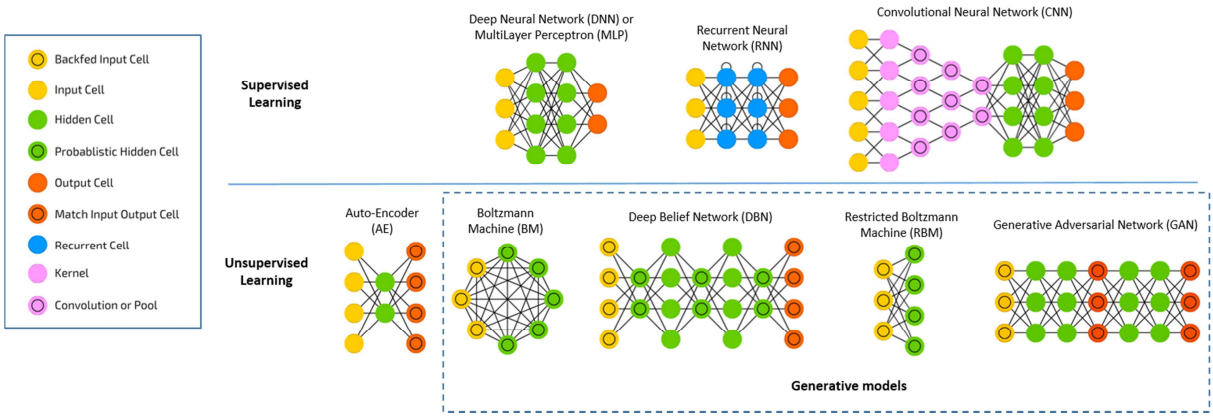

Fig. 7. Schematic representation of the most common network architectures in deep learning for radiotherapy applications (illustrations used with permission from [38] and classification inspired by [13]).

- A DNN is composed of several hidden layers in which all neurons of a layer i are connected to all the neurons of the i+1 layer. This simple architecture has the disadvantage of presenting a potentially slow learning process.
- A recurrent neural network (RNN) is suitable for the processing of temporally dependent information **[39]**. This is the type of network used for speech processing or video. Different from other types of deep networks, the idea here is to keep in mind the information previously processed, to help the network predict the succeeding data. The output y_t of the network is therefore a function not only of the input x_t at a time t but also of the inputs x_{t-i} at times t-i. The RNNs include long short-term memory (LSTM) and gated recurrent unit models.
- An auto-encoder (AE) is composed of a hidden layer of smaller size than the input one **[40]**. This hidden layer serves as an encoding layer for identifying a latent dominant structure of reduced

size with respect to the input signal. The neurons in the input layer are all connected to those in the hidden layer, all of which are connected to the output layer. When the encoding layer serves as input to another AE, it is called a stacked auto-encoder (SAE), which allows generating several levels of abstraction. Several variants have been proposed: stacked denoising (SDAE), sparse (SSAE), and variational (VAE). One of the advantages of this method is that it can be used in the context of unsupervised learning, which does not require labeled data.

- The Boltzmann machine (BM) is another unsupervised learning architecture. The objective is the same as in an AE (extract representations), but is based on a different statistical model. The connections between the neurons are bidirectional; therefore, a BM is comparable to a so-called generative model, which can generate new input data during learning. In a standard BM, all the neurons are connected to each other, whereas only the neurons of distinct layers are connected in a restricted Boltzmann machine (RBM) **[41]**.
- Deep belief network (DBNs) are essentially SAEs in which the encoding layers are replaced by RBMs **[42].** Only the two deepest layers have bidirectional connections. The training is performed in an unsupervised manner, except for the final adjustment of the network parameters performed in a supervised manner by adding a classification layer at the output of the network. The deep Boltzmann machine (DBM) is the equivalent of DBN, but with bidirectional connections between the neurons of each layer .
- The architecture of generative adversarial networks (GANs) is based on two models: a generative model G that produces synthetic data, and a discriminant model D that estimates the probability that these data are part of the training data **[43].** The goal of the process is to enable the G model to fool D.
- CNN is the DL architecture used by Krizhevsky et al. in 2012 (see discussion above). This architecture is widely used currently in image processing, for example, in automatic segmentation or computer-aided diagnostic in medical images. This is why we detail it more precisely in the next section.

2.3 Convolutional neural networks

Description

In a fully connected neural network, each neuron's output of a given layer is connected to an input node of every neuron in the succeeding layer, and neurons of the same layer are completely independent of each other. This is a very general-purpose connection pattern, as it makes no assumptions about the features in the data. However, information contained in medical images is generally spatially structured. One can notice that neighboring pixels corresponding to the same anatomical structure share similar intensity characteristics, which means that a specifically parameterized patch of neurons might be able to detect each pixel corresponding to the same structure. Furthermore, because the location of the structure searched is variable from one patient to another (lesions such as metastases for example) and from one image to another (due to differences in acquisition conditions), their location in the corresponding images will differ. Hence, the previously mentioned patch of neuron should have some type of invariance in spatial location in order to behave in the same way on the entire image. CNNs are specifically designed to take advantage of this spatially structured information.

CNN procedures have several advantages over most standard medical computer vision systems comprising manually engineered static programs [44]. Standard image features representations include scale-invariant feature transform (SIFT), histogram of oriented gradients (HoG), textons, spin images, and so forth. Identifying the right set of attributes most relevant to the problem addressed is often difficult and time-consuming and requires expert knowledge. Furthermore, the interaction between the characteristics of the environment might not be completely understood at the design

stage, or the amount of knowledge might be too large and complex for explicit encoding. Thus, CNNs now outperform these algorithms.

CNNs are the most common DL-based networks applied to image analysis. They were popularized after their stunning results in the ImageNet competition [36]. A CNN consists of several successive layers of data processing, whose aim is to find representative features of the input image, first simple, then more elaborate as the layers succeed each other (see Fig. 8). CNNs belong to the unsupervised or supervised learning category or both, depending on their architecture.

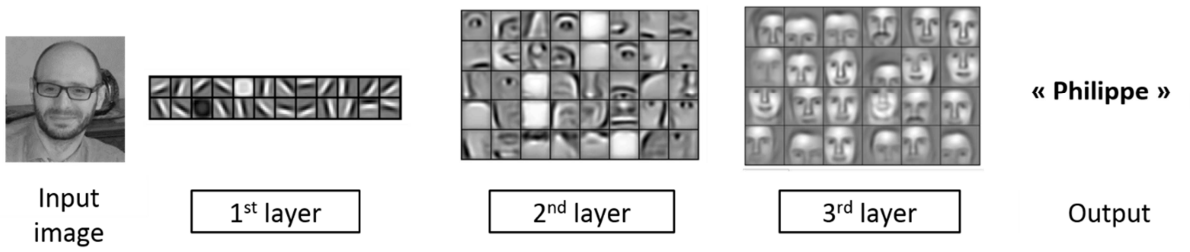

Fig. 8. Schematic illustration of the role of each layer of a CNN used for face recognition [42] (used with permission). The upper layers represent simple geometries (edges, lines). When the layers are deeper, simple features assemble to form shapes that are more complex.

To better understand how this architecture works, let us take the example in Fig. 9, where the image to be analyzed is composed of 6 × 6 pixels that can take individually different gray level values (for simplicity, values -1, 0, and 1). The coordinates of the pixels of the image can be written in the form (x, y), with x the line and y the column number. Square a filter, here consisting of 3 × 3 pixels, whose values are fixed arbitrarily (for the moment), in the upper left corner of the image to be analyzed, centering it on pixel (2, 2). Multiply the value of each pixel (x, y) of the image with each corresponding pixel (x, y) of the filter, sum the values obtained, divide it by the number of pixels of the operation (in our case 9), and apply the result to pixel (2, 2) of a new image, called a *feature map* (FM). Then, drag this filter one column to the right, in order to center it on pixel (2, 3) of the image to be analyzed, and carry out the same operation, which makes it possible to assign a value to pixel (2, 3) of the FM. The dragging operation of the window of one column to the right is often referred to as *stride = 1*. By thus sweeping the entire image, it is possible to recreate an entire new image (except the border): this operation is qualified as a *convolution*, from which the CNNs derive their name. The role of this transformation is to detect local features in different parts of an image, preserving the spatial information of the input.

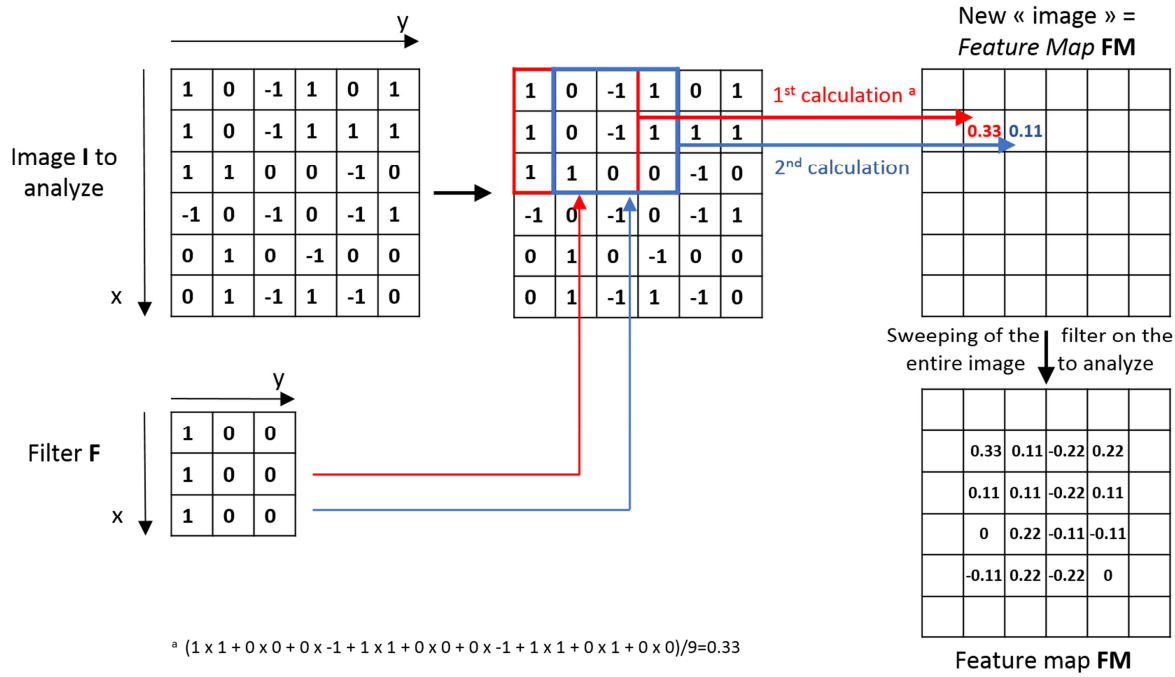

Fig. 9. Convolution operation applied to an image.

If this operation is transposed into a schematic representation of the neural networks, the pixel values can be seen as the input signals, and the filter values as the synaptic weights (see Fig. 10). Note that the filter F is often referred to as a *kernel*. In the previous example, the values of the filters (and thus weights) are set arbitrarily. In reality, we have already seen that the network iteratively adjusts these values during the training phase, so that the different layers can effectively extract characteristic representations of the input image. The convolution of the image by the kernel F, which produces the FM, constitutes a layer of the neural network. The multiple hidden layers of a CNN therefore represent successive convolution operations: the input data are the pixels of the image to be analyzed for the first layer, and those of the FM for the subsequent layers. Each layer actually includes several filters: in the example given in Fig. 11, the first layer consists of three different filters of size 3 × 3, the resulting FM being composed of three images (depth = 3). The next layer consists of four filters of size 3 × 3 and depth 3, which, convoluted with the FM of layer 1, produces an FM of depth 4.

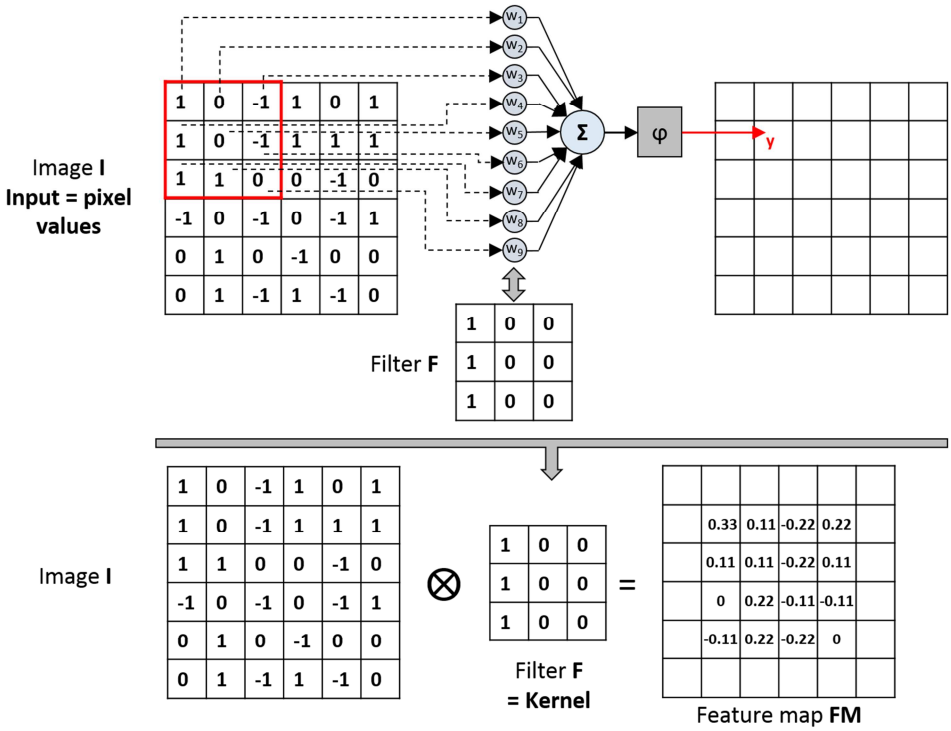

Fig. 10. Schematic representation of a convolution operation by a neural network.

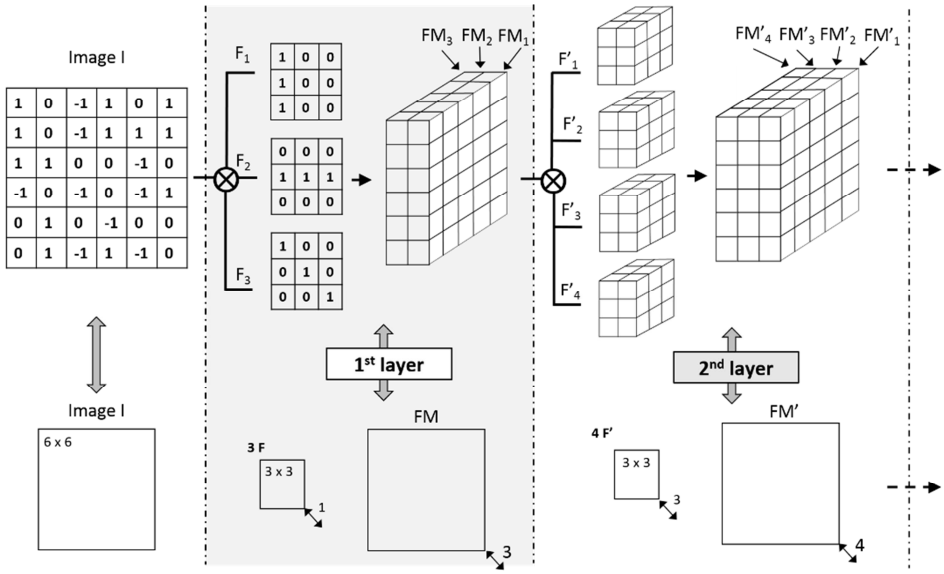

Fig. 11. Illustration of convolution operations performed in the first two hidden layers of a CNN. The lower part of the image is a synthetic view of the upper part.

Pooling

Practically in contemporary CNN, each convolutional layer is composed of dozens of grids of different weighted filters. Because an image is composed of tens of thousands of pixels, the number of operations required for CNN becomes important. To reduce this number and the computing load, it is common to insert a so-called pooling layer between two convolution layers. The role of this layer is

to reduce the size of the FM produced by the previous convolution layer. The classic technique of max pooling is to keep only the value of the largest pixel in a certain area, to maintain the characteristic of the image. Fig. 12 illustrates a max pooling operation performed on the FM of our previous example. With a filter of dimension 2 × 2 (not to be confused with the filters of the convolution operations), this operation consists here of keeping only the pixel whose value is maximum in an area defined by a matrix of dimension 2 × 2. This matrix is moved here by two pixels (stride = 2), and sweeps the whole area of the image. FM thus passes in this example from 16 to 4 pixels.

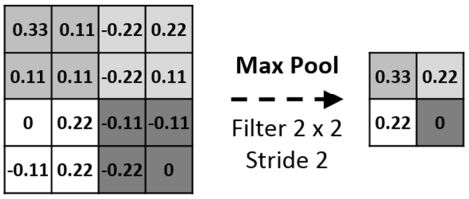

Fig. 12. Example of a max pooling filter of dimension 2 × 2 and stride = 2.

We have so far focused on 2D images. To exploit the actual 3D nature of many medical images, 3D CNNs have been developed, which calculate 3D FMs from 3D kernels. To reduce the degree of complexity and computation time of these models, 2.5D (or tri-planar) CNNs have been developed, in which the 3D volume is decomposed into axial, sagittal, and coronal views [45]. However, with the rapid improvement of computing power on GPUs, 3D CNNs could prevail in the future.

Better understanding through an example of CNN: AlexNET

We have seen that the basic structure of a CNN consists of alternating convolution and pooling layers. We have not mentioned it so far, but a nonlinearity operation such as ReLU is implicit after each layer. Around this basic scheme, many variants have been proposed depending on the type of application. The AlexNet network discussed earlier is shown in Fig. 13. Its function is image classification: from a 2D input image, it assigns a probability output to each of the thousand classes proposed in the competition. It consists of five layers of convolution, three layers of pooling, and three fully connected layers as output. The first layer is composed of 96 filters of dimension 11 × 11 × 1, applied to the input image with a stride = 4. The first resulting FM, of dimension 55 × 55 × 96, is taken as input of the second layer and convolved with 256 filters of size 5 × 5 × 96. After a max-pooling operation (3 × 3, stride = 2), the dimension of the second FM is 27 × 27 × 256. These operations are repeated until the last convolution layer generates an FM of size 13 × 13 × 256. After a last pooling operation that reduces the size of the FM to 6 × 6 × 256 (not shown in the figure), three fully connected layers follow each other. In contrast to convolutional layers that aim to detect patterns by successively scanning different parts of the image, the fully connected layers simultaneously take as input all the pixels of the FM. The first fully connected layer is composed of 9216 neurons and generates a 4096 × 1 × 1 size vector. At the output, a mathematical function called softmax transforms this vector of 4096 values into a probability vector of dimension 1000 × 1 × 1, which assigns a probability to each of the 1000 classes used.

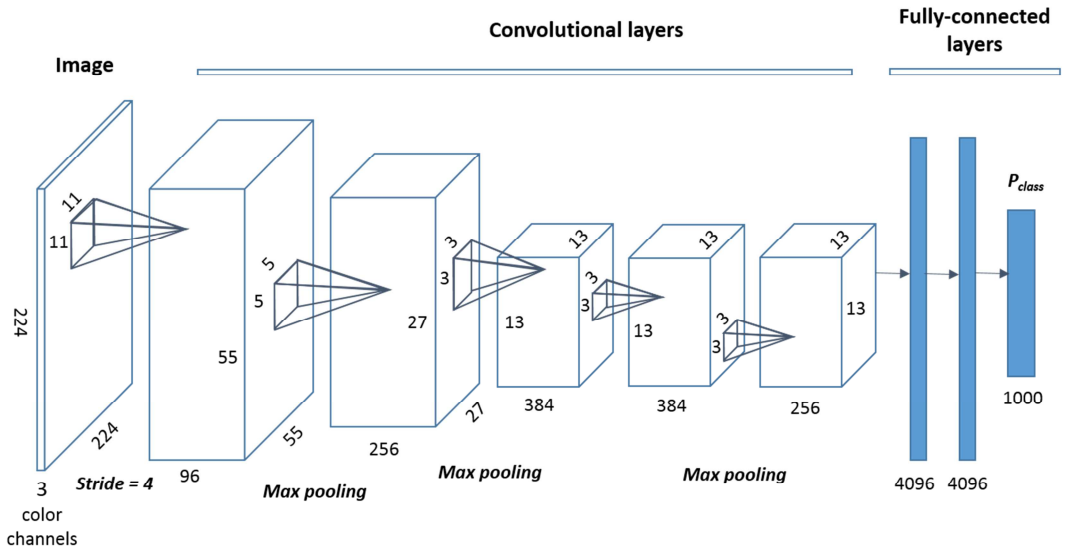

Fig. 13. Schematic representation of the AlexNet network (from [46]).

Other examples of CNN

In addition to AlexNET, other CNNs have been the subject of different variants, depending on specific applications. Among other outstanding networks, Visual Geometry Group (VGG) is characterized by a very simple structure (only convolution filter size 3 × 3 and pooling size 2 × 2) and by a significant depth of at least 16 layers [47]. It was developed for image classification, and performs on the concept that a DNN is more powerful when it is deeper. If the last fully connected layers of a CNN are deleted, you obtain a fully convolutional network (FCN), usually dedicated to segmentation tasks. The idea is to keep spatial information, increasing it in a last layer of sufficiently large size. However, after many layers of pooling, the final resolution is potentially low. To work around this problem, the U-net network, which was also developed for segmentation tasks, is proposed to add to the first convolutional part a second symmetrical part in which the pooling layers are replaced by interpolation layers [48]. The resolution of the output image is thus improved. Another application, deconvnet networks such as ZF-NET allowed a better understanding of how the network operates at each layer [49].

3. Deep learning methods applied to the radiotherapy workflow

Many teams are now developing DL methods that could straightforwardly be applied to one of the steps of the radiotherapy workflow (see Fig. 14). We made a review of the literature, and chose to classify the papers into seven categories relevant to these different radiotherapy steps: images used for radiotherapy planning and treatment set-up, image segmentation, computer-aided detection and diagnosis, image registration, treatment planning, motion management/patient setup during treatment, and data extraction and outcome prediction in radiotherapy. A synthesis of these DL applications in radiotherapy is proposed as presented in Table 2.

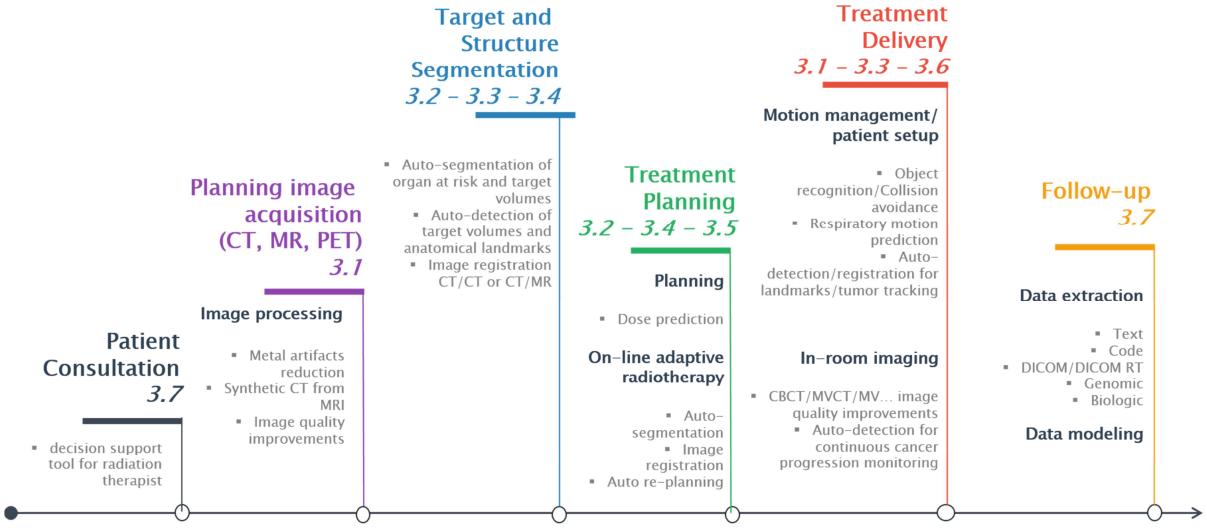

Fig. 14. Potential applications of deep learning approaches in the radiotherapy workflow. Numbers 3.1 to 3.7 refer to the sections in this article.

3.1 Images used for radiotherapy planning and treatment setup

Radiotherapy planning images are used to segment OAR and the target volume, and to plan the treatment. In order to calculate the dose delivered to the patient, it is necessary to provide the electronic tissue density to the algorithms used by the treatment planning systems (TPS). Through a simple calibration between electronic density and Hounsfield number, this density can be directly estimated from the CT planning imagery, which is the reference imaging for dosimetric calculation in radiotherapy [50]. Because MRI has some advantages in soft tissue contrast for several cancers (brain, prostate, etc.), it would be desirable to substitute this CT planning scan by an MRI planning scan [51]. However, due to the need of estimating the electron density, a standard CT planning scan is still acquired in addition to the MRI scan [52]. To overcome this limitation, a solution is to generate synthetic CT (sCT) images from MRI [53].

Radiotherapy treatment step	Application	Input data	DL-based method	Reference
Images used for radiotherapy planning and treatment setup	Pseudo X-ray image synthesis	MRI	U-net, Residual net, Cascaded refinement net	[54]
	Pseudo CT image synthesis	MRI	U-net, VGG	[55]
			FCN	[56]
			GAN	[57]
			Deep embedding CNN	[58]
	Pseudo MRI synthesis	CT	FCN	[59]
	Pseudo 7T MRI synthesis	3T MRI	CNN	[60]
	MR spectroscopic images (MRSI) artifact correction	MRSI	CNN	[61]
	Image artifact reduction	CT	CNN	[62,63]
	Spatial resolution improvement	Images	Super resolution CNN	[64]
	Image denoising	Synthetic CBCT	2D CNN	[65]
		On-board radiotherapy fluoroscopic X-rays	CNN, SAE	[66]
		CT	CNN	[67]
		CT	GAN	[68]
	Image prediction for limited-angle tomography	CT	CNN	[69]
Image segmentation	Portal vein	CT	2.5D CNN	[70,71]

	Brain glioma	MRI	CNN, U-net, FCN	[72]
			CNN	[73]
			3D CNN	[74,75]
			Holistically nested network	[76]
	Brain metastases	MRI	3D CNN	[77,78]
	Brain structures	MRI	DNN	[79]
		MRI	2.5D CNN	[37]
	Multi-age brain structures	MRI	CNN	[80]
	Brainstem	MRI	SDAE	[81]
	Hippocampus	MRI	DNN	[82]
		MRI	U-net	[83]
	Optic structures	MRI	SDAE	[84]
		CT	3D CNN	[85]
	Subcortical structures	MRI	3D CNN	[86]
		MRI	2.5D CNN	[87]
	Neuroanatomy structures	MRI	3D CNN	[88]
		MRI, US	2D, 2.5D, 3D CNNs	[89]
	Breast tissue	MRI	U-net	[90]
	Prostate	MRI	SAE, SSAE	[91]
		MRI	FCN	[92]
		CT	CNN	[93]
	Thoracic organs	CT	FCN	[94]
		CT	FCN	[95,96]
		CT	CNN	[97]
	Head and neck (H&N) organs	CT	2.5D CNN	[98]
	Esophagus	CT	3D CNN	[99]
	Abdominal organs	CT	3D CNN	[100]
	Spine	CT	CNN, FCN	[101]
	Liver and/or hepatic metastases	CT	Deep deconvolutional NN (DDNN)	[102]
		CT	FCN	[103]
		CT	3D CNN	[104]
		CT	CNN	[105]
		MRI, CT	FCN	[106]
	Rectal cancer and organs	CT	Deep dilated CNN	[107]
	Skin cancer	Dermoscopic images	CNN	[108]
	Rectal Cancer	MRI	CNN	[109]
	Bladder Cancer	CT	CNN	[110]
	Liver tumor	CT	CNN	[111]
	Nasopharyngeal tumor	CT	DDNN	[112]
	Nasopharyngeal tumor	MRI	CNN	[113]
	Oropharyngeal tumor	CT	CNN	[114]
	Tumor	Positron emission tomography (PET) -CT	CNN	[115]
Computer-aided detection	Pulmonary nodules	CT	3D CNN	[116]
		CT	CNN	[117]
		CT	CNN	[118]
		CT	CNN	[119]
		CT	CNN	[120]
	Prostate cancer	MRI	SAE	[121]
	Brain Metastases	MRI	CNN	[78,122]
	Brachytherapy catheters	MRI	(planned)	[123]
	L3 vertebra	CT	CNN	[124]
	Specific CT slice	CT	CNN	[125]
	Bone metastases	CT	CNN	[126]
	Specific vertebra	MRI	CNN	[127]
	Specific vertebra	US	CNN, SAE	[128,129]
	Carotid artery bifurcation	CT	DNN	[130]
	Anatomic landmarks	MRI, US, CT	CNN	[131]
	Brain, prostate landmarks	MRI, CT	CNN	[132]
Computer-aided diagnostic	Skin cancer	Images	CNN	[133]
	Pulmonary nodules	CT	DBN, CNN	[134]
		CT	AE	[135]
		CT	CNN, DNN, SAE	[136]
		CT	CNN, DBN, SDAE	[137]
		CT	CNN	[138]
	Breast cancer	Mammography	CNN	[139]

		Mammography	CNN	[140]
	Prostate cancer	MRI	DNN, VGG	[141]
	Rhabdomyosarcomas subtype	MRI	CNN	[142]
Image registration	Deformation prediction	MRI	VGG	[143]
	X-ray 2D/3D registration	Fluoroscopic X-rays	CNN	[144]
	2D/3D registration initialization	Fetal MRI	CNN	[145]
	MRI/MRI registration	MRI	SAE	[146]
	CT/MRI registration	CT,MRI	DNN	[147]
	X-ray 2D/3D registration	CBCT, 2D X-rays	FCN	[148]
Treatment planning	Predict dose from organ structures	RT Struct, RT Dose	U-net, CNN	[149]
		RT Struct, RT Dose	AE	[150,151]
Motion management/patient setup during treatment	Motion correction alignment setup with a soft robot activator	Motion capture camera images	MLP, RNN, LSTM	[152]
	Real-time, markerless, tumor-contouring to prevent mistracking on X-ray fluoroscopy	Fluoroscopic X-rays	CNN	[153]
	Intra- and inter-fractional variation prediction of lung tumors	Cyberknife breathing signal	NN	[154]
	Collision avoidance	3D camera images	Not described	[155]
Data extraction and outcome prediction in radiotherapy	Local failure after lung stereotactic body radiotherapy (SBRT)	CT, clinical risk factors (CRF)	DNN	[156]
	Survival risk after rectal cancer chemo-radiotherapy	PET-CT, survival rate	CNN	[157]
	Quality of life after prostate SBRT	Dose Volume Histogram, quality of life scores	DNN	[158]
	Rectum toxicity after cervical cancer brachy/radiotherapy	RT dose, Toxicity scores	VGG	[159]
	Survival rate for lung and H&N patients	CT	DNN	[160]
	Automated radiation adaptation in lung cancer	Clinical, genetic, dosimetric, PET data	GAN, CNN	[161]
	Medical image classification	24 organs on MRI, CT, PET	CNN	[162]
	Named entity recognition in clinical text	Electronic health records	DNN	[163]
	Clinical relation extraction	CRF	SAE	[164]

Table 2. Summary of the different deep learning based applications by radiotherapy treatment step.

Different methods have been developed in recent years [165] and a commercial solution has been recently evaluated on 170 prostate cancer patients [166]. CNNs appear to be one of the most promising methods for sCT generation. Han et al. proposed a novel U-net-based algorithm, the encoding part being based on the VGG 16-layer model [55]. Owing to transfer learning, they achieved a very satisfactory performance with limited training data (only 15 training subjects). They obtained a mean absolute error of 85 HU as compared to 95 HU for a standard atlas-based method. Another advantage is the processing time, which is approximately a few seconds for DL as compared to several minutes for the standard methods. However, the method generates each slice independently, resulting in potential discontinuity in the sCT [58]. Nie et al. proposed a 3D FCN for estimating CT images from MRI, while exploring different activation functions [56]. When tested on a pelvic phantom, they showed a better performance than three widely used approaches, with a 42.4 HU mean absolute error versus 48.1 to 66.1 for the other approaches. Wolterink et al. showed that a GAN can be trained to synthesize sCT with unpaired CT and MR images, avoiding the issue of misalignment between paired images [57]. They found that the model trained using unpaired data

outperformed the model trained using paired data. Xiang et al. developed an original “deep embedding” CNN to synthesize sCT [58]. The embedded blocks help fill the large gap between MRI and CT appearance and speed up the mapping. They demonstrated that their network performance is superior to three conventional and one CNN approaches on brain and prostate cases with reduced processing time. Stimpel et al. compared the use of three DL-based architecture (U-net, residual net, and cascade refinement network) to generate X-ray from MR projections, but so far, only on phantom images [54]. Note that the generation of synthetic images is not always done from MRI to CT. Actually, Zhao et al. proposed a whole brain segmentation method for CT images that first uses a DL network to synthesize an MRI from a CT image and then uses the synthetic MRI for segmentation [59].

Magnetic resonance spectroscopic image (MRSI) is a promising tool to detect metabolites within tissues, notably for glioblastoma and prostate cancer management in radiotherapy [167]. However, the presence of spectral artifacts is a problem in the routine clinical workflow. Gurbani et al. developed a CNN to identify poor-quality spectra and filter out artifacts with a high degree of sensitivity and specificity [61].

Artifacts on CT images related to the presence of metals in patients (dental fillings, spinal implants, hip prostheses, etc.) are problematic in radiotherapy. Actually, they can interfere with radiation diagnoses during the segmentation step and bias the calculation of the dose. To overcome these issues, many metal artifact reduction (MAR) algorithms have been proposed [168,169]. Recently, Gjesteby combined a CNN with an MAR into the image reconstruction process to achieve additional correction in critical image region, such as those with multiple metal objects [62,63]. Their results indicated that deep networks are valuable tools for improving or even replacing state-of-the-art MAR algorithms.

These DL image processing methods for both the generation of sCT from MRI and the correction of metallic implant artifacts involve learning a mapping from an image to another. This general concept could naturally be extended to other applications such as improving image quality, removing artifacts related to patient movements, synthesizing other image contrasts, or implementing rapid image acquisition strategies [170]. For example, Dong et al. used what they called a super resolution CNN method, which learns a mapping between low-/high-resolution images to restore image quality [64]. While these methods could be applied to radiotherapy planning images, they have also a great potential for image guided radiation therapy (IGRT) techniques to set up the patient during treatment. IGRT techniques are commonly based on X-ray (kilovoltage, megavoltage, cone beam CT (CBCT), megavoltage CT), MR, or ultrasound (US) imaging [171–173]. To reduce noise artifacts in CBCT images produced by a Leksell Gamma Knife Icon (Elekta, Sweden), Afshaq investigated the use of CNNs [65]. He showed that the proposed method outperforms conventional algorithms at the cost of a much higher computational time. These findings were only proved on synthetic CBCT images. To the best of our knowledge, the only one who used clinical IGRT images is Mori. He tested several types of deep CNN and AE models to process 430 X-ray images acquired on prostate cancer patients with oblique fluoroscopic units during patient setup procedure [66]. With a standard desktop computer, he achieved real-time image processing at 30 frames per second, including contrast enhancement and image denoising. Other DL methods originally developed for conventional diagnostic images could also have potential applications to IGRT images. For example, Bahrami et al. trained a CNN to reconstruct 7T-like images from 3T MRI, providing improved resolution and contrast [60]. This could be particularly useful for improving MR images produced by recent low-field MR systems (from 0.35 to 1.5 T) integrated into radiotherapy devices [174]. Concerning CT imaging, Zhang et al. developed a CNN to reduce artifacts produced by filtered back projection methods conducted on limited CT angle acquisition ranging from 130° to 170° [69]. This may be applicable on CBCT image acquisition, where limited angle acquisition is used to reduce the acquisition time and delivered dose. Reducing imaging dose delivered during IGRT is indeed a critical point, evidenced by

an accident in France, where 409 prostate patients received 8 to 10% overexposure due to excessive portal imaging controls, leading to the death of two of them after grade 4 rectal fistula [175]. In this context, deep CNN methods such as those developed by Chen et al. may be useful [67]. Their CNN, trained to match low-dose CT images toward normal-dose CT images, showed a better performance for noise reduction than iterative reconstruction and post-reconstruction processing. Yang et al. proposed a GAN to denoise low-dose CT images [68]. Compared to a CNN-based method, their method helped avoid the over-smoothing effect, but at the cost of losing critical features. All these methods have the potential to reduce the dose delivered during X-ray imaging used to localize patient during radiotherapy treatments.

3.2 Image segmentation

For each patient treated with radiotherapy, the radiation oncologist delineates slice by slice the target volume and the OAR on the planning images (CT or MR scans). Even if this task remains mainly manual in clinical routine, automated medical image segmentation plays an increasing role to help doctors in delineating anatomical structures or tumor regions. Many automatic segmentation methods have been explored, with varying degrees of success depending on the type of application or imagery studied [176,177]. There are now more than a dozen commercial segmentation software dedicated to radiotherapy, integrated or not into TPS [3].

Automatic segmentation is a frequent application of DL. The literature on this subject is already very broad, and our objective is not to be exhaustive, but rather to show that various published works can be applied to all radiotherapy indications. Nearly all the regions of human anatomy are concerned: cerebral, H&N, thoracic, abdominal, or pelvic. Different types of medical data are used for the segmentation of anatomical structures by DL, including MRI and CT images that are the reference imaging modalities for radiotherapy.

MRI is mostly used to investigate soft tissues and is the gold standard for the segmentation of the cerebral structures. Akkus et al. recently reviewed the numerous brain MRI segmentation methods involving DL [178]. The authors listed the most popular quantitative measures of brain segmentation quality, and the main brain segmentation challenges, including the multimodal brain tumor segmentation challenge (BraTS) [179]. This annual challenge dedicated to the automatic segmentation of gliomas since 2012 makes available a large database of multimodal MRI, composed in 2017 of 262 MRI for glioblastomas and 199 MRI for low-grade gliomas [180]. The availability of such large database partly explains why glioma is one of the most studied tumors for automatic segmentation by DL [73,75]. As highlighted by Isis et al. in their review on MRI-based brain tumor segmentation, DL methods can actually be considered as the current state-of-the-art method for glioma segmentation [181]. Tested on the 2013 BraTS dataset, Havaei et al. demonstrated that their CNN architecture outperforms the currently published state-of-the-art one, while being over 30 times faster [73]. With their CNN network called DeepMedic, Kamnitsas et al. obtained top ranking performance on BraTS 2015 [74]. Furthermore, the authors demonstrated the generalization capabilities of systems such as DeepMedic, which can be applied without significant modifications to other segmentation tasks such as for brain injuries and ischemic stroke, while still outperforming the state-of-the-art methods. In 2017, Kamnitsas et al. merged three DNN architectures to segment brain tumors on MRI: their CNN DeepMedic, two versions of U-net, and three fully connected networks. With this robust model, they won the first position in the BraTS final testing stage among more than 50 competing teams [72]. Zhuge et al. have proposed a new holistically nested neural network, and stated that it outperforms the classical CNN method for MRI-based glioma segmentation [76]. Compared to this many works concerning gliomas, BM have only very rarely been the subject of segmentation methods by DL. Liu et al. obtained competitive results with a CNN-based segmentation

method for BM on MRI, although the partial use of the BraTS database in their validation and test sets led to nuances in their conclusions [77].

The segmentation of brain OAR on MRI by DL methods has also been the subject of several studies. Brebisson et al. were the first to segment the whole brain into 134 anatomical regions using DNN [79]. Pai et al. worked on the same dataset of Brebisson and obtained equivalent results, but they also observed that the performance of their tri-planar CNN was inferior to standard methods, notably because of the lack of training cases [37]. Moeskoeps et al. designed a unique CNN network to precisely segment brain outlines regardless of age (prenatal, 23, and 70 years old) [80]. They also showed that this network could straightforwardly be applied to segment other anatomical regions while improving the results of Brebrisson. Other studies used SDAE, U-net or CNN to focus on a given structure, such as the brainstem [81] or the hippocampus [82,83], or on a group of structures such as those located in the optic region (optic nerve, chiasm, and pituitary) [84] or in the subcortical regions [86,87], and simultaneously up to 25 to 26 regions of the neuroanatomy [88,89]. While Milletari et al. compared different types of CNN architectures [89], Wachinger et al. used a 3D CNN to segment 25 brain structures with statistically significant improvements over several state-of-the-art methods, although the results were not as clear for subcortical structures [88]. Note that auto-segmentation of small volumes, such as optical structures (chiasm, optic nerves, etc.), is often difficult. To overcome this problem, 3D CNN with multi-scale patches (large patch to locate the tissue and small patch to label each voxel) has been developed with significantly better performance than the best scores reported in the literature [85].

MRI is also the reference modality for prostate segmentation, due in particular to the difficulty of differentiating on CT scans its contours with neighboring soft tissues in the base and apex regions [182]. Because prostate cancer is the most common cancer for men in developed countries [183], the automatic segmentation of this organ by DL has already been the subject of several studies. Guo et al. showed the superiority of their SAE model over state-of-the-art ones using handcrafted features, particularly on both anterior and posterior parts of the prostate [91]. Mehrtash et al. proposed an open-source toolkit called “DeepInfer” for developing DL models for different segmentation or detection tasks in medical imaging [184]. They tested their toolkit on prostate segmentation for targeted MRI-guided biopsy.

Many other organs can also be automatically segmented in MRI by DL. Google’s DeepMind Health has started a partnership with a hospital on H&N cancer to automatically segment tumor volumes and organs at risk on MRI scans [185]. Automated segmentation of breast and fibroglandular tissues may also be useful in radiotherapy, particularly because breast intensity modulated radiotherapy indications increased in recent years. Dalmis et al. showed that the U-net-based method they applied on MRI significantly outperformed existing algorithms in breast segmentation [90]. Christ et al. used an open-source DL framework to build a cascaded FCN model, which combined the segmentation of the liver and of hepatic lesions on MRI, and obtained results that compete with state-of-the-art methods [106]. They also showed that their method could be generalized to segment the liver and lesions on CT images.

While MR imaging has become the gold standard for organ segmentation of certain indications in radiotherapy, CT remains as the reference imaging modality (explained in Section 3.1). Several teams developed DL segmentation methods on CT images for various anatomical regions. Zhou et al. segmented 19 organs from different regions of the human anatomy on CT images, obtaining equivalent results to those of state-of-the-art methods with the advantage of using a single FCN architecture for all organs [94]. With a CNN dedicated to H&N cancers, Ibragimovic et al. segmented 9 organs, including 4 structures in the optic region [98]. They compared their findings not only with methods from academic research, as is generally the case with the studies cited in this paragraph, but also with three commercial software used in radiotherapy departments (VelocityAI 2.6.2, MIM 5.1.1, and ABAS 2.0 systems). They observed that DL methods demonstrate a superior or comparable

performance to the commercial software for all organs at risk, except for chiasm and submandibular glands. The esophagus, which is a structure with heterogeneous appearance and complex shape, was automatically and successfully segmented on public CT images from the "Multi-Atlas Labeling Beyond the Cranial Vault Challenge" with a 3D CNN developed by Fechter et al. They evaluated their method on the Synapse dataset, and showed that it outperformed all existing approaches [99]. Trullo et al. proposed an FCN framework for the joint segmentation of thoracic OAR, namely the heart, esophagus, trachea, and aorta. They obtained competitive results, particularly by accounting for relationship between these organs [95,96]. Hu et al. achieved an accuracy comparable to state-of-the-art methods with much higher efficiency for segmentation of the liver, spleen, and both kidneys [100]. By evaluating their automatic liver segmentation method on two public datasets of CT images (MICCAI-Sliver07 and 3Dircabd), Lu et al. showed that it demonstrates a superior segmentation accuracy than most of state-of-the-art methods [104]. Ben Cohen et al. and Yuan et al. developed several CNN and FCN approaches to automatically segment the liver on CT images and detect the lesions in the liver segmentation [102,103]. Still, for liver segmentation, Qin et al. proposed an original approach based on a CNN pipeline working with superpixels and an additional boundary class [105]. It achieved superior performance in comparison with U-net, CNN, and classical approaches. To better assess toxicity after SBRT, Ibragimovic et al. proposed a tri-planar CNN to segment and annotate portal vein on CT images [70,71]. Vania et al. combined a CNN and an FCN to automatically segment the spine on CT images [101]. Their results were better compared to those of conventional results, but slightly worse than those of U-net. The prostate can also be automatically segmented from CT using a CNN and multi-atlas fusion with satisfactory results [93].

DL methods were not only used to segment OAR, but also recently target volumes. Men et al. developed a CNN-like network to simultaneously segment abdomino-pelvic risk organs and the clinical target volume (CTV) of rectal cancers [107]. CNN were developed to segment oropharyngeal and nasopharyngeal CTV respectively on CT and MRI images, with close agreement when compared to inter-observer variability [113,114]. Other applications for segmentation of target volumes are presented in Section 3.5.

Medical Image Computing and Computer Assisted Intervention (MICCAI) has organized one of the first tumor delineation segmentation challenge in PET images [115]. Thirteen methods where implemented by challengers, and a CNN was ranked first. Automatic DL segmentation methods have also been developed for imaging modalities that are usually not used in the radiotherapy segmentation step. Automatic skin lesion segmentation in dermoscopic images, for example, is an important research field in dermatology, but may also help to define the target volume when treating skin lesions in radiotherapy. Experimental results show that CNN-based methods outperform other state-of-the-art dermoscopic segmentation algorithms [186,187]. US was also the subject of automatic segmentation attempts by CNN, for example for brain structures [89]. Automatic US image segmentation by DL could be useful in radiotherapy. Actually, patient or organ monitoring can be performed in some cases by US during treatment delivery [188–190]. This is also the case in prostate brachytherapy, where US endo-rectal imaging is used to monitor the procedure [191].

Despite these numerous DL automatic segmentation methods, there are few evaluations of their actual clinical contribution. The work of Lustberg et al. is one of the first to have evaluated the clinical interest of a commercial DL segmentation software prototype (Mirada DLC Expert prototype, Mirada Medical Ltd., United Kingdom). In a clinical radiotherapy context, they quantified the segmentation time using this software prototype for the segmentation of 6 thoracic OAR on CT, and compared those of manual contouring and atlas-based commercial automatic contouring [97]. The median time was 20 min for manual, 12.2 min for atlas-based, and 10 min for DL-based contouring.

3.3 Computer-aided detection (CADe) and diagnosis (CADx)

Although the concept of computer-aided medical image analysis appeared in the 1960s, the first developments on this subject began in the early 1980s [192]. Computer-aided medical image analysis can be divided into two categories: computer-aided detection (CADe) and diagnosis (CADx) [193]. The goal of a CADe system is to identify the location of organs, tumors, anatomical regions, or medical equipment in the images, and to help the medical staff for specific tasks. The objective of a CADx system is to provide medical information for the classification of a disease. Currently, automatic detection and diagnosis based on medical images have become a major research subject in the medical field. Esteva et al., for example, have recently developed a CNN that is capable of classifying skin cancer with a performance similar to that of dermatologists, and stated that it could be implemented on standard smartphones [133]. Even if a robust prospective validation in a blinded clinical trial must be undertaken in this particular example to ensure that this smartphone application is not harmful [194], DL technology opens promising perspectives for medical image analysis.

3.3.a Computer-aided diagnosis

Classifying pulmonary nodules on CT images according to their benign or malignant nature is a difficult task, and many teams have developed tools whose performances are regularly compared in challenges, such as the recent LungX Challenge [195]. One of the first studies that applied DL techniques to the problem of pulmonary nodule classification on CT images was performed by Hua et al., who showed that a combined DBN-CNN framework outperformed CADx systems relying on conventional handcrafted feature [134]. Since then, several authors developed other DL algorithms for this purpose. Ali et al. developed a reinforcement learning-based model for a CNN [120]. Kumar et al. proposed to use deep features extracted from an AE network combined with a binary decision tree as a classifier [135]. Song et al. compared the performances of three deep networks (CNN, DN and SAE) for lung cancer classification [136] : the CNN achieved the best performances. Sun et al. developed and compared the performances of three multichannel deep structured algorithms (CNN, DBN, and SDAE) and a classical handcrafted algorithm [137]. The best performance was obtained with the CNN. Instead of using CT images, Wang et al. recently tried to classify lung nodules from PET images, and compared a DL method with four classical machine learning methods. They showed that the performance of their CNN was not significantly different from the best classical methods, but that this performance could be improved by incorporating diagnostic features [138].

Breast cancer is the most common cancer in women worldwide [183], and one of the most treated with radiotherapy. Breast cancer CADx is therefore a crucial task, and CNN approaches were recently implemented for analyzing mammography images [139,140]. MRI has also been the subject of various works related to DL-based CADx algorithms. By finishing 4th place on the ProstateX challenge (classification of clinically significant prostate lesions on MRI), Chen et al. demonstrated that public state-of-the-art DL models such as VGG-16 could quickly and efficiently be retrained with limited data [141]. By analyzing multiparametric MRI, Banerjee et al. presented a CNN-based CADx for the classification of rhabdomyosarcoma subtypes [142].

3.3.b. Computer-aided detection

In their systematic review of articles published in December 2014 dealing with CADe of pulmonary nodules on CT images, Valente et al. stated that the latest techniques have not yet overcome all the

challenges of this task, mainly because of high FP per patient rates [193]. Nevertheless, none of the articles cited by Valente et al. relies on DL methods. Anirudh et al. were one of the first to explore lung nodule detection on CT images using 3D CNN, achieving a sensitivity of 60% for 3 FP per scan [116]. Roth et al. proposed a CNN method that improved the state-of-the-art CADe systems, with a mediastinal lung node sensitivity of 70% for 3 FP per patient [117]. Recently, all currently reported results on mediastinal lung nodule detection were surpassed with a CNN architecture adapted from the complex GoogLeNet model, achieving an 86% sensitivity and 3 FP per patient [118]. Teramoto et al. also concluded that CNN can be employed for FP detection rate reduction, showing that their method eliminates approximately half of the FPs as compared to a previous study concerning lung nodule detection on PET/CT [119].

Despite the high incidence of BM that affect up to one third of cancer patients, few detection DL-based methods have been published to date. Losch et al. were the first, to our knowledge, to use a CNN to detect BM on MRI [122]. They explored several kernel sizes and network depths, and observed that their network performances are comparable to the conventional state-of-the-art ones. Odelin et al. that it was possible to adapt an existing CNN (DeepMedic) to detect BM on multimodal MRI [78]. They used real and virtual patients, and obtained 98% sensitivity with only 7.2 false positive per patient. Sunwoo et al. developed a handcrafted feature-oriented CAD of BM on MRI, and used a simple one hidden layer ANN as the final FP discrimination method [196]. What is interesting is that they evaluated their CAD system in a clinical context, and showed that their CAD helps radiologists improve their diagnostic performance in the detection of BM on MRI, particularly for less-experienced reviewers.

Zhu et al. proposed an SAE method for detection of prostate cancer regions using multi-parametric MRI. They achieved a better performance than the conventional handcrafted features, with the advantage of directly identifying cancer regions from the entire prostate, compared to conventional prostate cancer detection methods that identify cancer only in specific regions of interest [121]. An original use of DL algorithms on MRI is the detection of catheters for brachytherapy, which are difficult to distinguish from neighboring tissues. In their work, Mastmeyer et al. used classical handcrafted features to detect and segment these brachytherapy catheters from MRI, but stated that they have begun investigating the training of DL networks [123].

An interesting application of CADe for radiotherapy is the automatic detection of anatomical landmarks. As stated before, this could be a valuable aid in preventing, for example, the delineation or treatment of wrong target, or in tracking a particular part of the anatomy. A good example is the level labeling of vertebra, which is an error-prone task because of the high-appearance similarity between consecutive vertebrae. CNN-based systems have been developed for detecting a particular slice on CT images, which achieved an average localization error of 4.8 mm for the third lumbar vertebra (L3) [125,197]. Again on CT images, a deep CNN was used to detect sclerotic metastases (bone lesions), while reducing the FP detection rate [126]. MRI can also be used to detect vertebrae. The CNN proposed by Forsberg et al. showed a detection accuracy on T1 and T2 images of less than 2.6 mm for lumbar and cervical vertebrae, with a labeling accuracy of 97.0% [127]. CNN and SAE were also proposed for the identification of the vertebra level on US images. Compared to matches of manually selected labels, DL matches of predicted vertebral level were correct in 94% of cases [128,129]. Originally developed for percutaneous needle insertion procedures, this type of application could also be applied to non-ionizing patient position monitoring during radiotherapy treatments. Other landmark detection methods performed by CNN could be used to assess the correct localization of the patient on various imaging modalities, such as carotid artery bifurcation on CT images [130], mitral annulus on US images [131], or apical/basal cardiac slices on MRI [132].

CADe and CADx algorithms are mainly useful in the medical diagnosis phase and do not at first glance directly concern radiotherapy. Nevertheless, these methods could find their place in the radiotherapy workflow in many cases. For example, automatic detection tools could help to control the positioning or to track in real time tumors/organs while the treatment is delivered. It could also support the radiation oncologist during the delineation stage by identifying anatomical landmarks such as the vertebral level. It might also open up new opportunities for exploiting the daily positioning images, for instance, by automatically screening for new metastases or identifying tumor progression/regression.

3.4 Image registration

Image registration is defined as the mathematical transformations applied to an image to make it correspond to a reference image. Registration methods are available in almost all radiotherapy software used to manage images. The American Association of Physicists in Medicine recently reviewed current approaches in radiotherapy [198]. In their survey about medical image registration techniques, Viergever et al. reviewed the developments that took place between 1998 and 2016 [199]. They observed major trends, notably that intensity-based techniques and rigid methods are now forming the basis of the vast majority of registration in clinical practice, and that registration use has progressed particularly in radiotherapy. They also concluded that it is unlikely that mutual information will be able to maintain its popularity, and that DL approaches applied to image registration could be the new challenger that could definitively make image registration fully integrated into routine clinical imaging.

DL algorithms have been proposed just to make the images comparable before using intensity-based methods for registration and to directly estimate the transformation parameters. Yang et al. proposed a DL network to predict image deformation, tested on 2D and 3D MRI datasets [143]. They achieved an equivalent prediction accuracy compared to state-of-the-art methods, with a significant speed-up of 1500x/66x respectively for 2D and 3D image registration. Miao et al. developed a CNN-based method for real-time 2D/3D registration, trained on synthetic data only [144,148]. They tested their method on three clinical applications (total knee arthroplasty, virtual implant planning system, and X-ray echo fusion), by registering X-ray images from fluoroscopic videos with 3D models. Results showed that their CNN method is very fast as it is capable of real-time registration at 10 fps, and significantly outperforms intensity-based methods. They also recently proposed a new FCN-based training strategy, and succeeded to reduce training time and improve registration robustness against artifacts [148]. A CNN approach was proposed by Hou et al. to solve the 2D/3D initialization problem in imaging applications, where the patient is moving during acquisition, such as fetal MRI [145]. Integrated into a full motion compensation framework, their method allowed to efficiently correct highly motion-corrupted scans. An unsupervised-based SAE network developed by Wu et al. for MRI registration consistently demonstrated a better performance compared to state-of-the-art methods [146]. The authors also showed that their proposed framework was quickly and efficiently adaptable to 7.0 T MRI, for which existing deformable methods developed for 3.0 T MRI did not work well. Ma et al. proposed a multimodal DNN-based registration algorithm to register real-time patient depth images with pre-operative CT or MRI [147]. Even if these applications are not directly related to radiotherapy, this type of DL method could be used during the treatment delivery, for example, by matching the kV or MV real-time images with the 3D model.

3.5 Treatment planning

Radiotherapy treatment planning aims to determine the optimal irradiation parameters (number of beams/arcs, multileaf collimator conformation/modulation, etc.). This planning is carried out using dedicated software (TPS) and is still currently mainly driven by the human user. However, many semi- or fully automated planning methods have been developed for several years, with the aim of reducing planning time while improving the quality of treatment plans. Some of them have been recently integrated and successfully tested in commercial solutions [200–203]. They mainly use machine learning methods that are trained on existing treatment plans [204–207]. DL methods are therefore applicable to the problem of automated treatment planning. To date, there are few published works in which a DL scheme is proposed to facilitate the radiotherapy planning task. Mardani et al. proposed a deep AE-based relation map between dose and structure that is learned from a dataset of 115 previously treated intensity-modulated radiotherapy (IMRT) prostate patients, allowing to predict achievable dose from the structures segmented on the planning images [150,151]. As compared to the state-of-art knowledge-based planning schemes, this novel predictive model has the advantage of being independent from patient and tumor site variability. Nguyen et al. proposed the same type of model, and used a U-net architecture with additional CNN layers to predict dose from structures [149]. The PTV, bladder, body, left and right femoral heads, and rectum structures of 80 IMRT prostate patients were used to train the model, as well as the 2D dose map of the central PTV slice. They obtained an average mean and maximum dose differences of all structures within 2.3% of the prescription dose.

If we deviate a bit from the heart of the planning process itself, the DL approaches for automatic segmentation and image registration, which we have described in the previous sections, are particularly adapted to the specific workflow of adaptive radiotherapy (ART). ART is defined as a radiotherapy treatment process, where the treatment plan can be modified using a systematic feedback of measurements performed during treatment [208]. The ART process can be applied in real-time conditions, while the patient is on the bed inside the treatment room [209–211]. In this case, the DL approaches for automatic segmentation and image registration, which are potentially faster than standard approaches, could allow reduction of the patient treatment time. The DL accuracy performance in terms of automatic segmentation can also prove to be useful in the ART process. Trebeschi et al. showed that a CNN can improve the speed and accuracy of diffusion weighted MRI-based rectal cancer segmentation [109]. Another example of potential application is bladder cancer. Segmentation of bladder cancer is crucial, because monitoring its volume variation during neoadjuvant chemotherapy is used to predict treatment outcome. One can envision that it may also be useful for ART to monitor changes during the course of treatment. Cha et al. developed a CNN model to automatically segment the bladder cancer region on CT images, which showed a better performance than another method they have developed beforehand [110]. Vivanti et al. described a CNN-based method to quantify liver tumor burden on longitudinal CT scans [111]. Men et al. developed the DDNN method to segment nasopharyngeal gross tumor volume and CTV on planning CT, outperforming a VGG-based model [112]. These four examples of DL-based segmentation illustrate applications that could take place in the ART process. Nevertheless, they were tested on high-quality images compared to those used for patient positioning in radiotherapy with IGRT. To our knowledge, no DL segmentation approach has yet been applied to these types of images, thus opening up interesting research perspectives.

3.6 Motion management/patient setup during treatment

Managing intra- and inter-fraction patient and organ motion has become a central topic in contemporary medical physics research, stimulated by the technical realization and subsequent clinical implementation of hybrid beam delivery [212–214]. Machine learning techniques have been used for many years [215], and DL approaches have now also been investigated in this area. Ogunmolu et al. developed a soft-robot actuator to position patients in maskless H&N radiotherapy. Combined with two Kinect cameras and a single inflatable air bladder, it allowed to track the patient's face and to control the soft robot, achieving 2.5 mm accuracy in head positioning [216,217]. Originally based on a linear quadratic Gaussian feedback model, the authors developed several deep architectures (MLP, RNN, and LSTM) that they planned to use with their soft-robot motion alignment system [152]. Respiratory tumor motion management is also a challenging task, particularly because stereotactic lung radiotherapy techniques have become popular [218]. To predict intra- and inter-fractional variation in lung tumor location, Park et al. developed a neural network with embedded fuzzy logic systems trained on breathing data of 130 patients collected on a Cyberknife facility [154]. Their framework allowed estimating the next breathing signal before the next incoming signal arrives. Compared to existing methods, it improved the prediction accuracy, while reducing the computational time by a factor of more than 100. With an average processing time of 1.5 ms, it could achieve real-time prediction and can therefore help in improving tracking techniques. Terunuma et al. developed a CNN-based contouring method to track tumors in real-time on X-ray fluoroscopy [153]. They validated their method on simulated fluoroscopic images, achieving a 30 frames per second processing time.

Wrong patient positioning is a potential pitfall in radiotherapy treatment, which could lead to mis-irradiation or patient collision with the gantry. Using a set of 3D cameras placed inside the treatment room, Santhanam et al. developed a DL-based system to automatically detect potential patient safety hazards during the radiotherapy setup [155]. Three-dimensional objects such as the gantry and bed were first recognized and classified, and a DL framework was used to analyze these objects, allowing the system to recognize wrong patient or accessory setup.

Finally, as already mentioned in previous sections, DL segmentation, detection, or registration algorithms have an interesting potential for motion management in radiotherapy including the tracking of structures on imaging systems used to control patient positioning.

3.7 Medical data extraction and outcome prediction in radiotherapy

Currently, many medical records are numerically collected from patients treated with radiotherapy, such as administrative (codes), genomics, clinical (text), biological (blood tests, cardiac tests, etc.), diagnostic/simulation imaging (DICOM), and treatment plan data (DICOM RT plan, structures and dose, DICOM positioning control images) [219]. This information is often referred to as EHR or big data in the literature, which are concepts that evolved continuously in recent years [220,221].

These data represent a considerable source of new medical knowledge, if they could be analyzed on a large scale. The goal is to link the patient's disease, its treatment, and its clinical effects, in order to design decision-making tools that will help the physician to better orient and personalize the patient therapy. In order to achieve this, algorithms should be first designed to extract intelligible data to provide inputs to other algorithms that model the clinical effects in a second step.

Several DL methods have already been applied to extract medical information, reviewed recently by Shickel et al. [13]. As examples at different levels of data extraction, Qayyum et al. proposed a CNN framework to retrieve and classify multimodal medical images (MR, CT, PET) for 24 body organs, obtaining a 99.77% accuracy [162]. Wu et al. developed a DNN model to recognize clinical texts in

medical documents, which outperformed state-of-the-art methods [163]. Other DL methods have been developed for identifying and extracting the relation existing between patient medical problems, treatments, and tests ("clinical relation extraction"). Tested on the i2b2 relation challenge dataset [222], Lv et al. proposed an SAE-based relation classification model [164]. They showed that their model performed better than one based on the original word features. Therefore, even if these studies have not been carried out directly in relation to radiotherapy, they are applicable to the extraction of the majority of data useful for radiotherapy predictive modeling (text, codes, DICOM).

Multiple radiation oncology research groups have shown the value of machine learning methods for predicting radiotherapy outcomes, although clinical adoption is going slow due to the huge barrier of understanding these complex models by clinicians [223–225]. The prediction of radiation toxicities has, for example, been studied with machine learning techniques for several diseases such as lung [226], prostate [227], or H&N cancer [228]. Meanwhile, many DL methods have been applied to the analysis of medical data (including outcome prediction), and have already been the subject of recent reviews [13,14]. DL methods appear indeed to be promising for outcome prediction in radiotherapy. In prostate radiotherapy big data analytics, Coates et al. stated that DL strategies may prove to be useful in the case of radiation-induced biological effects, given the complexity of the physical and biological processes involved [229]. Concerning neuroblastoma, a pediatric cancer disease that is in some cases irradiated, Salazar et al. emphasized the fact that a genetic approach alone is unlikely to yield fruitful drug discovery, as there are very rare recurrent somatic mutations detected in this disease [230]. That is why DL approaches, which can integrate more sophisticated data generated from patients and animal models, may be best suited to model the complexity of neuroblastoma etiology. Muthalaly et al. demonstrated that DL networks can be trained to predict mortality in acute lymphoblastic leukemia, a childhood disease for which radiotherapy may be used as part of treatment [231]. Nevertheless, no consistent work combining DL methods and modeling of radiotherapy clinical effects has been published until early 2017 [219]. Since then, several authors have tried to model, using very different DL-based approaches, the risks associated with radiotherapy treatments. Zhen et al. demonstrated that a pre-trained CNN is able to model rectum dose distribution and predict rectum toxicity after cervical cancer radiotherapy [159]. They showed that transfer learning might overcome the difficulty to train a CNN from scratch, as patient sample size is often small. Jochem et al. learned a three-layer DNN model on radiomic features for survival prediction in lung and H&N cancers [160]. Although they did not observe a superior performance compared to that of conventional modeling strategies, they demonstrated that DL methods represent a major advantage because feature selection is no longer a required component. To predict local failure following SBRT, Aneja et al. merged a CNN and a DNN to analyze respectively patient CT simulation and CRF. They showed that DNN could improve the predictive ability compared to logistic regression [156]. Li et al. also used imaging data to predict survival risks for rectal cancer patients. They used the biological target volume from PET-CT as training data for a CNN, and stated that their model could predict the tumor recurrence risk better than current models [157]. To predict quality of life (QOL) in urinary and bowel domains after prostate SBRT, Qi et al. proposed a DNN model trained with DVH data [158]. They showed that their model was able to predict the QOL scores with ± 5 points. A combination of three learning components (GAN, DNN, and deep Q-network) was proposed by Tseng et al. to build an autonomous clinical decision support system for a response-based ART [161]. Using clinical, genetic, and radiomic features, their framework allowed to adapt patient dose per fraction in a response-adapted treatment setting.

3.8 Summary

We reviewed publications in which DL approaches were applied in radiotherapy. We observed that all steps of patient workflow in radiotherapy were related, to a greater or lesser degree, to potential applications of DL. Automatic segmentation of medical structures is, for example, already widely discussed in the literature, for all locations and for many imaging modalities. However, there have been few studies on tumor delineation, for which there is still considerable room for improvement. It should be noted that the automatic delineation of tumors has applications during the treatment planning stage as well as during adaptive radiotherapy, for example, to automatically monitor the evolution of tumor lesions through patient positioning images.

We believe that these images, made during radiotherapy treatments to control patient positioning, are indeed an important source of inspiration for DL applications. They are available in large numbers because several images can be made during each treatment fraction, and patient treatments usually comprise about thirty fractions. One disadvantage of these images is that they are generally of poorer quality than diagnostic images; we have noted that the first publications regarding improvement of their quality by DL methods have been published recently. Regarding this application of positioning images, DL could make a major contribution through some CADx and CADe techniques that are currently used for diagnosis. For example, DL could assist in the detection of new metastases during treatment or the development of new tracking techniques. Patient motion management is indeed a problem in which there is still much room for improvement in the context of radiotherapy, in which the very first applications of DL methods were published. There have been very few studies on DL applications for treatment planning published to date, while the dosimetric databases are widespread and quite easily exploitable. Finally, concerning the use of DL for outcome prediction in radiotherapy, the first studies have been published recently, and the field of research on this subject remains vast and complex.

4. Deep learning criticisms

Despite their many advantages, DNNs have not been imposed much in clinical routine. One of the main criticisms is the lack of theory concerning DL and the fact that standard general principles are mostly empirically obtained. The choice of the general architecture of the network (the layout of the layers, their number, the size of filters, etc.) best suited to the problem to be solved is mostly guided by intuition and carried out experimentally. There are also some recognized tricks and tips for improving learning but without theory to justify them.

The true generalization capability of DNNs in image vision can also be questioned because they can be fooled [232]. Changing an image in a way imperceptible to humans can thus lead a DNN to label it as something entirely different. It is also possible to produce images that are completely unrecognizable to the human eyes but labeled with certainty by the neural network. It is therefore important to keep in mind that even if some DNNs can perform at near-human ability, the way they perceive and interpret the world is far different from the human way. Among other things, they lack explicit ways of representing causal relationships and of integrating abstract knowledge, which make them prone to error due to unavoidable finite and incomplete training set.

The need to build coherent and sufficiently large databases in the field of medicine is another challenge. Indeed, DNNs require a large diversity of training examples in order to be effective in real-world operation. This implies that neural networks need to be trained with a sufficient variety of representative examples to be able to capture the data underlying structure that allows them to generalize new cases. Another consequence is that a neural network trained on datasets collected

with biases (due to intra- or inter-expert variation for example) will certainly exhibit the same biases. Furthermore, when the algorithm is based on supervised learning, the classes of the patterns must be known as well, which requires extra effort from clinical experts. Rigorous collection of data is thus a critical and often underestimated and time-consuming part of DL (and machine learning in general). For example, in one of our previous works focused on brain metastases segmentation in multimodal MRI, the constitution of a database composed of information of 182 patients required nearly three months of work [78]. With current radiotherapy treatment planning systems each patient's data often still needs to be manually selected, restored, opened on the manufacturer's software, and then exported individually to obtain exploitable DICOM files.

This difficulty in building large databases has been noted in many of the publications cited above, in almost all categories in Section 3. Although the use of picture archiving and communication systems (PACS) in most western hospitals allows access to millions of medical images [5], many authors indicate for example that there is a lack of properly labeled imagery databases for the development of automatic segmentation methods based on DL [88, 104, 233]. Limited availability of datasets is also an issue for the further advancement of CAD, and building well annotated datasets seems at least as crucial as developing new algorithms [118]. This is particularly true if these methods have to be applied to low-quality images, such as those used to localize patient during IGRT procedures. As pointed out by Viergever et al., the development of registration-based DL methods may be hampered by one of the main obstacles to the implantation of registration techniques in medical imaging, namely, the lack of reference datasets for validation, and thus for learning [199]. Concerning outcome prediction, the road toward predictive radiotherapy by DL methods could still be long. It is first crucial that radiation oncologists should be able to understand the prediction of DL algorithms. However, these algorithms are still considered "black boxes", and their interpretation is often difficult [13]. About training, major challenges, such as heterogeneous data, non-standardized terminologies, and computer or workflow incompatibility will make the dream of big data research difficult in radiotherapy [234].

5. Conclusion

Several DL methods that can be applied to a step of the radiotherapy workflow have been recently published. Despite their promising results, we are probably, at this time, only at the prehistory of the use of these methods in radiotherapy. The number of applications and their performance will likely evolve rapidly in the coming years. The main obstacle to this development could be related to the lack of training data, as pointed out by many authors cited in this survey. We have tried to provide a number of ideas and perspectives to explore, but obviously, there are still many approaches to be developed and many applications to imagine in this exciting field of DL for radiotherapy.

Funding

This research did not receive any specific grant from funding agencies in the public, commercial, or not-for-profit sectors.

References

[1] I.E. Naqa, M.J. Murphy, What Is Machine Learning?, in: I.E. Naqa, R. Li, M.J. Murphy (Eds.), Mach. Learn. Radiat. Oncol., Springer International Publishing, 2015: pp. 3–11. doi:10.1007/978-3-319-18305-3_1.

[2] M. Feng, G. Valdes, N. Dixit, T.D. Solberg, Machine Learning in Radiation Oncology: Opportunities, Requirements, and Needs, Front. Oncol. 8 (2018). doi:10.3389/fonc.2018.00110.

[3] G. Sharp, K.D. Fritscher, V. Pekar, M. Peroni, N. Shusharina, H. Veeraraghavan, J. Yang, Vision 20/20: Perspectives on automated image segmentation for radiotherapy, Med. Phys. 41 (2014). doi:10.1118/1.4871620.

[4] Y. LeCun, Y. Bengio, G. Hinton, Deep learning, Nature. 521 (2015) 436–444. doi:10.1038/nature14539.

[5] G. Litjens, T. Kooi, B.E. Bejnordi, A.A.A. Setio, F. Ciompi, M. Ghafoorian, J.A.W.M. van der Laak, B. van Ginneken, C.I. Sánchez, A survey on deep learning in medical image analysis, Med. Image Anal. 42 (2017) 60–88. doi:10.1016/j.media.2017.07.005.

[6] D. Wu, N. Sharma, M. Blumenstein, Recent advances in video-based human action recognition using deep learning: A review, in: 2017 Int. Jt. Conf. Neural Netw. IJCNN, 2017: pp. 2865–2872. doi:10.1109/IJCNN.2017.7966210.

[7] I. El Naqa, K. Brock, Y. Yu, K. Langen, E.E. Klein, On the Fuzziness of Machine Learning, Neural Networks, and Artificial Intelligence in Radiation Oncology, Int. J. Radiat. Oncol. 100 (2018) 1–4. doi:10.1016/j.ijrobp.2017.06.011.

[8] L. Xing, E.A. Krupinski, J. Cai, Artificial intelligence will soon change the landscape of medical physics research and practice, Med. Phys. (2018). doi:10.1002/mp.12831.

[9] J.-G. Lee, S. Jun, Y.-W. Cho, H. Lee, G.B. Kim, J.B. Seo, N. Kim, Deep Learning in Medical Imaging: General Overview, Korean J. Radiol. 18 (2017) 570. doi:10.3348/kjr.2017.18.4.570.

[10] K. Suzuki, Overview of deep learning in medical imaging, Radiol. Phys. Technol. (2017) 1–17. doi:10.1007/s12194-017-0406-5.

[11] D. Shen, G. Wu, H.-I. Suk, Deep Learning in Medical Image Analysis, Annu. Rev. Biomed. Eng. 19 (2017) 221–248. doi:10.1146/annurev-bioeng-071516-044442.

[12] R. Miotto, F. Wang, S. Wang, X. Jiang, J.T. Dudley, Deep learning for healthcare: review, opportunities and challenges, Brief. Bioinform. (2017). doi:10.1093/bib/bbx044.

[13] B. Shickel, P.J. Tighe, A. Bihorac, P. Rashidi, Deep EHR: A Survey of Recent Advances in Deep Learning Techniques for Electronic Health Record (EHR) Analysis, IEEE J. Biomed. Health Inform. PP (2017) 1–1. doi:10.1109/JBHI.2017.2767063.

[14] D. Ravì, C. Wong, F. Deligianni, M. Berthelot, J. Andreu-Perez, B. Lo, G.Z. Yang, Deep Learning for Health Informatics, IEEE J. Biomed. Health Inform. 21 (2017) 4–21. doi:10.1109/JBHI.2016.2636665.

[15] I. Goodfellow, Y. Bengio, A. Courville, Deep Learning, MIT Press. (2016). http://www.deeplearningbook.org/.

[16] T. Zhou, G. Han, B.N. Li, Z. Lin, E.J. Ciaccio, P.H. Green, J. Qin, Quantitative analysis of patients with celiac disease by video capsule endoscopy: A deep learning method, Comput. Biol. Med. 85 (2017) 1–6. doi:10.1016/j.compbiomed.2017.03.031.

[17] Y. Bengio, Learning Deep Architectures for AI, Found. Trends® Mach. Learn. 2 (2009) 1–127. doi:10.1561/2200000006.

[18] D. Crevier, Ai: The Tumultuous History Of The Search For Artificial Intelligence, First Edition edition, Basic Books, New York, NY, 1993.

[19] J. McCarthy, P. Hayes, Some philosophical problems from the standpoint of artificial intelligence, Read. Plan. 393 (1969) 1–51.

[20] M.A. Boden, Artificial Intelligence and Natural Man, Basic Books, 1977.

[21] A.M. Turing, Computing machinery and intelligence, Mind. 59 (1950) 433–460.

[22] A. Newell, H. Simon, The logic theory machine–A complex information processing system, IRE Trans. Inf. Theory. 2 (1956) 61–79. doi:10.1109/TIT.1956.1056797.
[23] A.L. Samuel, Some Studies in Machine Learning Using the Game of Checkers, IBM J Res Dev. 3 (1959) 210–229. doi:10.1147/rd.33.0210.
[24] R.S. Michalski, J.G. Carbonell, T.M. Mitchell, Machine Learning: An Artificial Intelligence Approach, Springer Science & Business Media, 2013.
[25] P. Natarajan, J.C. Frenzel, D.H. Smaltz, Demystifying Big Data and Machine Learning for Healthcare, CRC Press, 2017.
[26] T.M. Mitchell, Machine Learning, McGraw-Hill, New York, 1997.
[27] M. Mohri, A. Rostamizadeh, A. Talwalkar, Foundations of Machine Learning, The MIT Press, 2012.
[28] K. M, V. Perumal, Performance evaluation and comparative analysis of various machine learning techniques for diagnosis of breast cancer., Biomed. Res. 27 (2016). http://www.alliedacademies.org/abstract/performance-evaluation-and-comparative-analysis-of-various-machine-learning-techniques-for-diagnosis-of-breast-cancer-4545.html (accessed April 19, 2018).
[29] R. Miotto, L. Li, B.A. Kidd, J.T. Dudley, Deep Patient: An Unsupervised Representation to Predict the Future of Patients from the Electronic Health Records, Sci. Rep. 6 (2016) 26094. doi:10.1038/srep26094.
[30] B. Mwangi, T.S. Tian, J.C. Soares, A review of feature reduction techniques in neuroimaging, Neuroinformatics. 12 (2014) 229–244. doi:10.1007/s12021-013-9204-3.
[31] A. Jalalimanesh, H. Shahabi Haghighi, A. Ahmadi, M. Soltani, Simulation-based optimization of radiotherapy: Agent-based modeling and reinforcement learning, Math. Comput. Simul. 133 (2017) 235–248. doi:10.1016/j.matcom.2016.05.008.
[32] N. Tajbakhsh, J.Y. Shin, S.R. Gurudu, R.T. Hurst, C.B. Kendall, M.B. Gotway, J. Liang, Convolutional Neural Networks for Medical Image Analysis: Full Training or Fine Tuning?, IEEE Trans. Med. Imaging. 35 (2016) 1299–1312. doi:10.1109/TMI.2016.2535302.
[33] F. Rosenblatt, The perceptron, a perceiving and recognizing automaton, Cornell Aeronaut. Lab. - Rep. 85-460-1. (1957). http://blogs.umass.edu/brain-wars/files/2016/03/rosenblatt-1957.pdf (accessed November 9, 2017).
[34] Y. Lecun, Une procedure d'apprentissage pour reseau a seuil asymmetrique (A learning scheme for asymmetric threshold networks), Cognitiva. 85 (1985) 599–604.
[35] D.E. Rumelhart, G.E. Hinton, R.J. Williams, Learning representations by back-propagating errors, Nature. 323 (1986) 323533a0. doi:10.1038/323533a0.
[36] A. Krizhevsky, I. Sutskever, G.E. Hinton, Imagenet classification with deep convolutional neural networks, in: Adv. Neural Inf. Process. Syst., 2012: pp. 1097–1105.
[37] S.K. Zhou, H. Greenspan, D. Shen, Deep Learning for Medical Image Analysis, Academic Press, 2017.
[38] F. van Veen, The Neural Network Zoo - http://www.asimovinstitute.org/neural-network-zoo/, Asimov Inst. (2016). http://www.asimovinstitute.org/neural-network-zoo/ (accessed November 10, 2017).
[39] T. Mikolov, M. Karafiát, L. Burget, J. Černockỳ, S. Khudanpur, Recurrent neural network based language model, in: Elev. Annu. Conf. Int. Speech Commun. Assoc., 2010.
[40] P. Baldi, Autoencoders, unsupervised learning, and deep architectures, in: Proc. ICML Workshop Unsupervised Transf. Learn., 2012: pp. 37–49.
[41] I. Sutskever, G.E. Hinton, G.W. Taylor, The Recurrent Temporal Restricted Boltzmann Machine, in: D. Koller, D. Schuurmans, Y. Bengio, L. Bottou (Eds.), Adv. Neural Inf. Process. Syst. 21, Curran Associates, Inc., 2009: pp. 1601–1608. http://papers.nips.cc/paper/3567-the-recurrent-temporal-restricted-boltzmann-machine.pdf.

[42] H. Lee, R. Grosse, R. Ranganath, A.Y. Ng, Convolutional deep belief networks for scalable unsupervised learning of hierarchical representations, in: Proc. 26th Annu. Int. Conf. Mach. Learn., ACM, 2009: pp. 609–616.
[43] I. Goodfellow, J. Pouget-Abadie, M. Mirza, B. Xu, D. Warde-Farley, S. Ozair, A. Courville, Y. Bengio, Generative adversarial nets, in: Adv. Neural Inf. Process. Syst., 2014: pp. 2672–2680.
[44] G. Antipov, S.-A. Berrani, N. Ruchaud, J.-L. Dugelay, Learned vs. Hand-Crafted Features for Pedestrian Gender Recognition, in: Proc. 23rd ACM Int. Conf. Multimed., ACM, New York, NY, USA, 2015: pp. 1263–1266. doi:10.1145/2733373.2806332.
[45] J. Bernal, K. Kushibar, D.S. Asfaw, S. Valverde, A. Oliver, R. Martí, X. Lladó, Deep convolutional neural networks for brain image analysis on magnetic resonance imaging: a review, ArXiv171203747 Cs. (2017). http://arxiv.org/abs/1712.03747.
[46] H. Wang, Y. Cai, Y. Zhang, H. Pan, W. Lv, H. Han, Deep Learning for Image Retrieval: What Works and What Doesn't, in: IEEE, 2015: pp. 1576–1583. doi:10.1109/ICDMW.2015.121.
[47] K. Simonyan, A. Zisserman, Very Deep Convolutional Networks for Large-Scale Image Recognition, ArXiv14091556 Cs. (2014). http://arxiv.org/abs/1409.1556.
[48] O. Ronneberger, P. Fischer, T. Brox, U-net: Convolutional networks for biomedical image segmentation, in: Int. Conf. Med. Image Comput. Comput.-Assist. Interv., Springer, 2015: pp. 234–241.
[49] M.D. Zeiler, R. Fergus, Visualizing and understanding convolutional networks, in: Eur. Conf. Comput. Vis., Springer, 2014: pp. 818–833.
[50] G.C. Pereira, M. Traughber, R.F. Muzic, The Role of Imaging in Radiation Therapy Planning: Past, Present, and Future, BioMed Res. Int. 2014 (2014) 1–9. doi:10.1155/2014/231090.
[51] A.M. Owrangi, P.B. Greer, C.K. Glide-Hurst, MRI-only treatment planning: benefits and challenges, Phys. Med. Biol. 63 (2018) 05TR01. doi:10.1088/1361-6560/aaaca4.
[52] M.A. Schmidt, G.S. Payne, Radiotherapy planning using MRI, Phys. Med. Biol. 60 (2015) R323–R361. doi:10.1088/0031-9155/60/22/R323.
[53] S.-H. Hsu, Y. Cao, K. Huang, M. Feng, J.M. Balter, Investigation of a method for generating synthetic CT models from MRI scans of the head and neck for radiation therapy, Phys. Med. Biol. 58 (2013) 8419. doi:10.1088/0031-9155/58/23/8419.
[54] B. Stimpel, C. Syben, T. Würfl, K. Mentl, A. Dörfler, A. Maier, MR to X-Ray Projection Image Synthesis, ArXiv171007498 Cs. (2017). http://arxiv.org/abs/1710.07498.
[55] X. Han, MR-based synthetic CT generation using a deep convolutional neural network method, Med. Phys. 44 (2017) 1408–1419. doi:10.1002/mp.12155.
[56] D. Nie, X. Cao, Y. Gao, L. Wang, D. Shen, Estimating CT Image from MRI Data Using 3D Fully Convolutional Networks, in: G. Carneiro, D. Mateus, L. Peter, A. Bradley, J.M.R.S. Tavares, V. Belagiannis, J.P. Papa, J.C. Nascimento, M. Loog, Z. Lu, J.S. Cardoso, J. Cornebise (Eds.), Deep Learn. Data Labeling Med. Appl., Springer International Publishing, 2016: pp. 170–178. doi:10.1007/978-3-319-46976-8_18.
[57] J.M. Wolterink, A.M. Dinkla, M.H.F. Savenije, P.R. Seevinck, C.A.T. van den Berg, I. Išgum, Deep MR to CT Synthesis Using Unpaired Data, in: Simul. Synth. Med. Imaging, Springer, Cham, 2017: pp. 14–23. doi:10.1007/978-3-319-68127-6_2.
[58] L. Xiang, Q. Wang, D. Nie, L. Zhang, X. Jin, Y. Qiao, D. Shen, Deep embedding convolutional neural network for synthesizing CT image from T1-Weighted MR image, Med. Image Anal. 47 (2018) 31–44. doi:10.1016/j.media.2018.03.011.
[59] C. Zhao, A. Carass, J. Lee, Y. He, J.L. Prince, Whole Brain Segmentation and Labeling from CT Using Synthetic MR Images, in: Mach. Learn. Med. Imaging, Springer, Cham, 2017: pp. 291–298. doi:10.1007/978-3-319-67389-9_34.
[60] K. Bahrami, F. Shi, I. Rekik, D. Shen, Convolutional Neural Network for Reconstruction of 7T-like Images from 3T MRI Using Appearance and Anatomical Features, in: Deep Learn. Data Labeling Med. Appl., Springer, Cham, 2016: pp. 39–47. doi:10.1007/978-3-319-46976-8_5.

[61] S.S. Gurbani, E. Schreibmann, A.A. Maudsley, J.S. Cordova, B.J. Soher, H. Poptani, G. Verma, P.B. Barker, H. Shim, L.A.D. Cooper, A convolutional neural network to filter artifacts in spectroscopic MRI, Magn. Reson. Med. (2018). doi:10.1002/mrm.27166.

[62] L. Gjesteby, Q. Yang, Y. Xi, Y. Zhou, J. Zhang, G. Wang, Deep learning methods to guide CT image reconstruction and reduce metal artifacts, in: Med. Imaging 2017 Phys. Med. Imaging, International Society for Optics and Photonics, 2017: p. 101322W. doi:10.1117/12.2254091.

[63] L. Gjesteby, Q. Yang, Y. Xi, B. Claus, Y. Jin, B. De Man, G. Wang, Reducing metal streak artifacts in CT images via deep learning: Pilot results, in: 14th Int. Meet. Fully Three-Dimens. Image Reconstr. Radiol. Nucl. Med., 2017: pp. 611–614.

[64] C. Dong, C.C. Loy, K. He, X. Tang, Image Super-Resolution Using Deep Convolutional Networks, IEEE Trans. Pattern Anal. Mach. Intell. 38 (2016) 295–307. doi:10.1109/TPAMI.2015.2439281.

[65] A. Ashfaq, Segmentation of Cone Beam CT in Stereotactic Radiosurgery, TRITA-STH, 2016:104, KTH, School of Technology and Health (STH)., 2016. http://kth.diva-portal.org/smash/record.jsf?pid=diva2:975179 (accessed September 28, 2017).

[66] S. Mori, Deep architecture neural network-based real-time image processing for image-guided radiotherapy, Phys. Med. 40 (2017) 79–87. doi:10.1016/j.ejmp.2017.07.013.

[67] H. Chen, Y. Zhang, W. Zhang, P. Liao, K. Li, J. Zhou, G. Wang, Low-dose CT via convolutional neural network, Biomed. Opt. Express. 8 (2017) 679–694. doi:10.1364/BOE.8.000679.

[68] Q. Yang, P. Yan, Y. Zhang, H. Yu, Y. Shi, X. Mou, M.K. Kalra, G. Wang, Low Dose CT Image Denoising Using a Generative Adversarial Network with Wasserstein Distance and Perceptual Loss, ArXiv170800961 Cs. (2017). http://arxiv.org/abs/1708.00961.

[69] H. Zhang, L. Li, K. Qiao, L. Wang, B. Yan, L. Li, G. Hu, Image prediction for limited-angle tomography via deep learning with convolutional neural network, ArXiv Prepr. ArXiv160708707. (2016). https://arxiv.org/abs/1607.08707 (accessed July 26, 2017).

[70] B. Ibragimov, D. Toesca, D. Chang, A. Koong, L. Xing, Combining deep learning with anatomical analysis for segmentation of the portal vein for liver SBRT planning, Phys. Med. Biol. 62 (2017) 8943–8958. doi:10.1088/1361-6560/aa9262.

[71] B. Ibragimov, D.A.S. Toesca, D.T. Chang, A.C. Koong, L. Xing, Deep Learning-Based Autosegmentation of Portal Vein for Prediction of Central Liver Toxicity After SBRT, Int. J. Radiat. Oncol. Biol. Phys. 99 (2017) E672.

[72] K. Kamnitsas, W. Bai, E. Ferrante, S. McDonagh, M. Sinclair, N. Pawlowski, M. Rajchl, M. Lee, B. Kainz, D. Rueckert, B. Glocker, Ensembles of Multiple Models and Architectures for Robust Brain Tumour Segmentation, in: Brainlesion Glioma Mult. Scler. Stroke Trauma. Brain Inj., Springer, Cham, 2017: pp. 450–462. doi:10.1007/978-3-319-75238-9_38.

[73] M. Havaei, A. Davy, D. Warde-Farley, A. Biard, A. Courville, Y. Bengio, C. Pal, P.-M. Jodoin, H. Larochelle, Brain Tumor Segmentation with Deep Neural Networks, Med. Image Anal. 35 (2017) 18–31. doi:10.1016/j.media.2016.05.004.

[74] K. Kamnitsas, E. Ferrante, S. Parisot, C. Ledig, A. Nori, A. Criminisi, D. Rueckert, B. Glocker, DeepMedic on Brain Tumor Segmentation, Athens Greece Proc BRATS-MICCAI. (2016).

[75] K. Kamnitsas, C. Ledig, V.F.J. Newcombe, J.P. Simpson, A.D. Kane, D.K. Menon, D. Rueckert, B. Glocker, Efficient multi-scale 3D CNN with fully connected CRF for accurate brain lesion segmentation, Med. Image Anal. 36 (2017) 61–78. doi:10.1016/j.media.2016.10.004.

[76] Y. Zhuge, A.V. Krauze, H. Ning, J.Y. Cheng, B.C. Arora, K. Camphausen, R.W. Miller, Brain tumor segmentation using holistically nested neural networks in MRI images, Med. Phys. 44 (2017) 5234–5243. doi:10.1002/mp.12481.

[77] Y. Liu, S. Stojadinovic, B. Hrycushko, Z. Wardak, S. Lau, W. Lu, Y. Yan, S.B. Jiang, X. Zhen, R. Timmerman, L. Nedzi, X. Gu, A deep convolutional neural network-based automatic delineation strategy for multiple brain metastases stereotactic radiosurgery, PloS One. 12 (2017) e0185844. doi:10.1371/journal.pone.0185844.

[78] O. Charron, A. Lallement, D. Jarnet, V. Noblet, J.-B. Clavier, P. Meyer, Automatic detection and segmentation of brain metastases on multimodal MR images with a deep convolutional neural network, Comput. Biol. Med. 95 (2018) 43–54. doi:10.1016/j.compbiomed.2018.02.004.

[79] A. de Brebisson, G. Montana, Deep neural networks for anatomical brain segmentation, in: Proc. IEEE Conf. Comput. Vis. Pattern Recognit. Workshop, 2015: pp. 20–28.

[80] P. Moeskops, M.A. Viergever, A.M. Mendrik, L.S. de Vries, M.J.N.L. Benders, I. Isgum, Automatic Segmentation of MR Brain Images With a Convolutional Neural Network, IEEE Trans. Med. Imaging. 35 (2016) 1252–1261. doi:10.1109/TMI.2016.2548501.

[81] J. Dolz, N. Betrouni, M. Quidet, D. Kharroubi, H.A. Leroy, N. Reyns, L. Massoptier, M. Vermandel, Stacking denoising auto-encoders in a deep network to segment the brainstem on {MRI} in brain cancer patients: A clinical study, Comput. Med. Imaging Graph. 52 (2016) 8–18. doi:http://dx.doi.org/10.1016/j.compmedimag.2016.03.003.

[82] M. Kim, G. Wu, D. Shen, Unsupervised Deep Learning for Hippocampus Segmentation in 7.0 Tesla MR Images, in: Proc. 4th Int. Workshop Mach. Learn. Med. Imaging - Vol. 8184, Springer-Verlag New York, Inc., New York, NY, USA, 2013: pp. 1–8. doi:10.1007/978-3-319-02267-3_1.

[83] L. Cao, L. Li, J. Zheng, X. Fan, F. Yin, H. Shen, J. Zhang, Multi-task neural networks for joint hippocampus segmentation and clinical score regression, Multimed. Tools Appl. (2018) 1–18. doi:10.1007/s11042-017-5581-1.

[84] J. Dolz, N. Reyns, N. Betrouni, D. Kharroubi, M. Quidet, L. Massoptier, M. Vermandel, A deep learning classification scheme based on augmented-enhanced features to segment organs at risk on the optic region in brain cancer patients, ArXiv170310480 Cs. (2017). http://arxiv.org/abs/1703.10480 (accessed April 10, 2017).

[85] X. Ren, L. Xiang, D. Nie, Y. Shao, H. Zhang, D. Shen, Q. Wang, Interleaved 3D-CNNs for joint segmentation of small-volume structures in head and neck CT images, Med. Phys. (n.d.). doi:10.1002/mp.12837.

[86] J. Dolz, C. Desrosiers, I.B. Ayed, 3D fully convolutional networks for subcortical segmentation in MRI: A large-scale study, NeuroImage. (2017). doi:10.1016/j.neuroimage.2017.04.039.

[87] K. Kushibar, S. Valverde, S. Gonzalez-Villa, J. Bernal, M. Cabezas, A. Oliver, X. Llado, Automated sub-cortical brain structure segmentation combining spatial and deep convolutional features, ArXiv170909075 Cs. (2017). http://arxiv.org/abs/1709.09075.

[88] C. Wachinger, M. Reuter, T. Klein, DeepNAT: Deep Convolutional Neural Network for Segmenting Neuroanatomy, NeuroImage. (2017). doi:10.1016/j.neuroimage.2017.02.035.

[89] F. Milletari, S.-A. Ahmadi, C. Kroll, A. Plate, V. Rozanski, J. Maiostre, J. Levin, O. Dietrich, B. Ertl-Wagner, K. Bötzel, N. Navab, Hough-CNN: Deep learning for segmentation of deep brain regions in MRI and ultrasound, Comput. Vis. Image Underst. 164 (2017) 92–102. doi:10.1016/j.cviu.2017.04.002.

[90] M.U. Dalmış, G. Litjens, K. Holland, A. Setio, R. Mann, N. Karssemeijer, A. Gubern-Mérida, Using deep learning to segment breast and fibroglandular tissue in MRI volumes, Med. Phys. 44 (2017) 533–546. doi:10.1002/mp.12079.

[91] Y. Guo, Y. Gao, D. Shen, Deformable MR Prostate Segmentation via Deep Feature Learning and Sparse Patch Matching, IEEE Trans. Med. Imaging. 35 (2016) 1077–1089. doi:10.1109/TMI.2015.2508280.

[92] F. Milletari, N. Navab, S.A. Ahmadi, V-Net: Fully Convolutional Neural Networks for Volumetric Medical Image Segmentation, in: 2016 Fourth Int. Conf. 3D Vis. 3DV, 2016: pp. 565–571. doi:10.1109/3DV.2016.79.

[93] L. Ma, R. Guo, G. Zhang, F. Tade, D.M. Schuster, P. Nieh, V. Master, B. Fei, Automatic segmentation of the prostate on CT images using deep learning and multi-atlas fusion, in: International Society for Optics and Photonics, 2017: p. 101332O. doi:10.1117/12.2255755.

[94] X. Zhou, T. Ito, R. Takayama, S. Wang, T. Hara, H. Fujita, Three-Dimensional CT Image Segmentation by Combining 2D Fully Convolutional Network with 3D Majority Voting, in: Deep

Learn. Data Labeling Med. Appl., Springer, Cham, 2016: pp. 111–120. doi:10.1007/978-3-319-46976-8_12.

[95] R. Trullo, C. Petitjean, S. Ruan, B. Dubray, D. Nie, D. Shen, Segmentation of Organs at Risk in thoracic CT images using a SharpMask architecture and Conditional Random Fields, in: 2017 IEEE 14th Int. Symp. Biomed. Imaging ISBI 2017, 2017: pp. 1003–1006. doi:10.1109/ISBI.2017.7950685.

[96] R. Trullo, C. Petitjean, D. Nie, D. Shen, S. Ruan, Joint Segmentation of Multiple Thoracic Organs in CT Images with Two Collaborative Deep Architectures, in: Deep Learn. Med. Image Anal. Multimodal Learn. Clin. Decis. Support, Springer, Cham, 2017: pp. 21–29. doi:10.1007/978-3-319-67558-9_3.

[97] T. Lustberg, J. van Soest, M. Gooding, D. Peressutti, P. Aljabar, J. van der Stoep, W. van Elmpt, A. Dekker, Clinical evaluation of atlas and deep learning based automatic contouring for lung cancer, Radiother. Oncol. J. Eur. Soc. Ther. Radiol. Oncol. (2017). doi:10.1016/j.radonc.2017.11.012.

[98] B. Ibragimov, L. Xing, Segmentation of organs-at-risks in head and neck CT images using convolutional neural networks, Med. Phys. 44 (2017) 547–557. doi:10.1002/mp.12045.

[99] T. Fechter, S. Adebahr, D. Baltas, I. Ben Ayed, C. Desrosiers, J. Dolz, Esophagus segmentation in CT via 3D fully convolutional neural network and random walk, Med. Phys. 44 (2017) 6341–6352. doi:10.1002/mp.12593.

[100] P. Hu, F. Wu, J. Peng, Y. Bao, F. Chen, D. Kong, Automatic abdominal multi-organ segmentation using deep convolutional neural network and time-implicit level sets, Int. J. Comput. Assist. Radiol. Surg. (2016) 1–13. doi:10.1007/s11548-016-1501-5.

[101] M. Vania, D. Mureja, D. Lee, Automatic Spine Segmentation using Convolutional Neural Network via Redundant Generation of Class Labels for 3D Spine Modeling, ArXiv171201640 Cs. (2017). http://arxiv.org/abs/1712.01640.

[102] Y. Yuan, Hierarchical Convolutional-Deconvolutional Neural Networks for Automatic Liver and Tumor Segmentation, ArXiv171004540 Cs. (2017). http://arxiv.org/abs/1710.04540.

[103] A. Ben-Cohen, I. Diamant, E. Klang, M. Amitai, H. Greenspan, Fully Convolutional Network for Liver Segmentation and Lesions Detection, in: Deep Learn. Data Labeling Med. Appl., Springer, Cham, 2016: pp. 77–85. doi:10.1007/978-3-319-46976-8_9.

[104] F. Lu, F. Wu, P. Hu, Z. Peng, D. Kong, Automatic 3D liver location and segmentation via convolutional neural network and graph cut, Int. J. Comput. Assist. Radiol. Surg. 12 (2017) 171–182. doi:10.1007/s11548-016-1467-3.

[105] W. Qin, J. Wu, F. Han, Y. Yuan, W. Zhao, B. Ibragimov, J. Gu, L. Xing, Superpixel-based and boundary-sensitive convolutional neural network for automated liver segmentation, Phys. Med. Biol. (2018). doi:10.1088/1361-6560/aabd19.

[106] P.F. Christ, F. Ettlinger, F. Grün, M.E.A. Elshaera, J. Lipkova, S. Schlecht, F. Ahmaddy, S. Tatavarty, M. Bickel, P. Bilic, others, Automatic Liver and Tumor Segmentation of CT and MRI Volumes using Cascaded Fully Convolutional Neural Networks, ArXiv Prepr. ArXiv170205970. (2017). https://arxiv.org/abs/1702.05970 (accessed February 27, 2017).

[107] K. Men, J. Dai, Y. Li, Automatic segmentation of the clinical target volume and organs at risk in the planning CT for rectal cancer using deep dilated convolutional neural networks, Med. Phys. (2017). doi:10.1002/mp.12602.

[108] Y. Yuan, M. Chao, Y.-C. Lo, Automatic Skin Lesion Segmentation Using Deep Fully Convolutional Networks With Jaccard Distance, IEEE Trans. Med. Imaging. 36 (2017) 1876–1886. doi:10.1109/TMI.2017.2695227.

[109] S. Trebeschi, J.J.M. van Griethuysen, D.M.J. Lambregts, M.J. Lahaye, C. Parmer, F.C.H. Bakers, N.H.G.M. Peters, R.G.H. Beets-Tan, H.J.W.L. Aerts, Deep Learning for Fully-Automated Localization and Segmentation of Rectal Cancer on Multiparametric MR, Sci. Rep. 7 (2017). doi:10.1038/s41598-017-05728-9.

[110] K.H. Cha, L.M. Hadjiiski, R.K. Samala, H.-P. Chan, R.H. Cohan, E.M. Caoili, C. Paramagul, A. Alva, A.Z. Weizer, Bladder Cancer Segmentation in CT for Treatment Response Assessment: Application of Deep-Learning Convolution Neural Network—A Pilot Study, Tomogr. J. Imaging Res. 2 (2016) 421–429. doi:10.18383/j.tom.2016.00184.

[111] R. Vivanti, A. Szeskin, N. Lev-Cohain, J. Sosna, L. Joskowicz, Automatic detection of new tumors and tumor burden evaluation in longitudinal liver CT scan studies, Int. J. Comput. Assist. Radiol. Surg. 12 (2017) 1945–1957. doi:10.1007/s11548-017-1660-z.

[112] K. Men, X. Chen, Y. Zhang, T. Zhang, J. Dai, J. Yi, Y. Li, Deep Deconvolutional Neural Network for Target Segmentation of Nasopharyngeal Cancer in Planning Computed Tomography Images, Front. Oncol. 7 (2017). doi:10.3389/fonc.2017.00315.

[113] Y. Wang, C. Zu, G. Hu, Y. Luo, Z. Ma, K. He, X. Wu, J. Zhou, Automatic Tumor Segmentation with Deep Convolutional Neural Networks for Radiotherapy Applications, Neural Process. Lett. (2018) 1–12. doi:10.1007/s11063-017-9759-3.

[114] C.E. Cardenas, R.E. McCarroll, L.E. Court, B. Elgohari, H. Elhalawani, C.D. Fuller, M. Jomaa, M.A.M. Meheissen, A.S.R. Mohamed, A. Rao, B. Williams, A. Wong, J. Yang, M. Aristophanous, Deep Learning Algorithm for Auto-Delineation of High-Risk Oropharyngeal Clinical Target Volumes with Built-in Dice Similarity Coefficient Parameter Optimization Function, Int. J. Radiat. Oncol. (2018). doi:10.1016/j.ijrobp.2018.01.114.

[115] M. Hatt, B. Laurent, A. Ouahabi, H. Fayad, S. Tan, L. Li, W. Lu, V. Jaouen, C. Tauber, J. Czakon, F. Drapejkowski, W. Dyrka, S. Camarasu-Pop, F. Cervenansky, P. Girard, T. Glatard, M. Kain, Y. Yao, C. Barillot, A. Kirov, D. Visvikis, The first MICCAI challenge on PET tumor segmentation, Med. Image Anal. (n.d.). doi:10.1016/j.media.2017.12.007.

[116] R. Anirudh, J.J. Thiagarajan, T. Bremer, H. Kim, Lung nodule detection using 3D convolutional neural networks trained on weakly labeled data, in: G.D. Tourassi, S.G. Armato (Eds.), 2016: p. 978532. doi:10.1117/12.2214876.

[117] H.R. Roth, L. Lu, J. Liu, J. Yao, A. Seff, K. Cherry, L. Kim, R.M. Summers, Improving Computer-Aided Detection Using Convolutional Neural Networks and Random View Aggregation, IEEE Trans. Med. Imaging. 35 (2016) 1170–1181. doi:10.1109/TMI.2015.2482920.

[118] H.C. Shin, H.R. Roth, M. Gao, L. Lu, Z. Xu, I. Nogues, J. Yao, D. Mollura, R.M. Summers, Deep Convolutional Neural Networks for Computer-Aided Detection: CNN Architectures, Dataset Characteristics and Transfer Learning, IEEE Trans. Med. Imaging. 35 (2016) 1285–1298. doi:10.1109/TMI.2016.2528162.

[119] A. Teramoto, H. Fujita, O. Yamamuro, T. Tamaki, Automated detection of pulmonary nodules in PET/CT images: Ensemble false-positive reduction using a convolutional neural network technique, Med. Phys. 43 (2016) 2821–2827. doi:10.1118/1.4948498.

[120] I. Ali, G.R. Hart, G. Gunabushanam, Y. Liang, W. Muhammad, B. Nartowt, M. Kane, X. Ma, J. Deng, Lung Nodule Detection via Deep Reinforcement Learning, Front. Oncol. 8 (2018). doi:10.3389/fonc.2018.00108.

[121] Y. Zhu, L. Wang, M. Liu, C. Qian, A. Yousuf, A. Oto, D. Shen, MRI-based prostate cancer detection with high-level representation and hierarchical classification, Med. Phys. 44 (2017) 1028–1039. doi:10.1002/mp.12116.

[122] Max Loschs, Thesis: Detection and Segmentation of Brain Metastases with Deep Convolutional Networks, 2015. http://www.diva-portal.se/smash/get/diva2:853460/FULLTEXT01.pdf (accessed October 26, 2016).

[123] A. Mastmeyer, G. Pernelle, R. Ma, L. Barber, T. Kapur, Accurate model-based segmentation of gynecologic brachytherapy catheter collections in MRI-images, Med. Image Anal. 42 (2017) 173–188. doi:10.1016/j.media.2017.06.011.

[124] S. Belharbi, C. Chatelain, R. Hérault, S. Adam, S. Thureau, M. Chastan, R. Modzelewski, Spotting L3 slice in CT scans using deep convolutional network and transfer learning, Comput. Biol. Med. 87 (2017) 95–103. doi:10.1016/j.compbiomed.2017.05.018.

[125] B.D. de Vos, M.A. Viergever, P.A. de Jong, I. Išgum, Automatic Slice Identification in 3D Medical Images with a ConvNet Regressor, in: Deep Learn. Data Labeling Med. Appl., Springer, Cham, 2016: pp. 161–169. doi:10.1007/978-3-319-46976-8_17.
[126] H.R. Roth, J. Yao, L. Lu, J. Stieger, J.E. Burns, R.M. Summers, Detection of Sclerotic Spine Metastases via Random Aggregation of Deep Convolutional Neural Network Classifications, in: J. Yao, B. Glocker, T. Klinder, S. Li (Eds.), Recent Adv. Comput. Methods Clin. Appl. Spine Imaging, Springer International Publishing, Cham, 2015: pp. 3–12. http://link.springer.com/10.1007/978-3-319-14148-0_1 (accessed January 16, 2017).
[127] D. Forsberg, E. Sjöblom, J.L. Sunshine, Detection and Labeling of Vertebrae in MR Images Using Deep Learning with Clinical Annotations as Training Data, J. Digit. Imaging. 30 (2017) 406–412. doi:10.1007/s10278-017-9945-x.
[128] J. Hetherington, V. Lessoway, V. Gunka, P. Abolmaesumi, R. Rohling, SLIDE: automatic spine level identification system using a deep convolutional neural network, Int. J. Comput. Assist. Radiol. Surg. (2017) 1–10. doi:10.1007/s11548-017-1575-8.
[129] J. Hetherington, M. Pesteie, V.A. Lessoway, P. Abolmaesumi, R.N. Rohling, Identification and tracking of vertebrae in ultrasound using deep networks with unsupervised feature learning, in: 2017: p. 101350K–101350K–7. doi:10.1117/12.2252641.
[130] Y. Zheng, D. Liu, B. Georgescu, H. Nguyen, D. Comaniciu, 3D deep learning for efficient and robust landmark detection in volumetric data, in: Int. Conf. Med. Image Comput. Comput.-Assist. Interv., Springer, 2015: pp. 565–572. http://link.springer.com/chapter/10.1007/978-3-319-24553-9_69 (accessed July 20, 2017).
[131] F.C. Ghesu, B. Georgescu, T. Mansi, D. Neumann, J. Hornegger, D. Comaniciu, An artificial agent for anatomical landmark detection in medical images, in: Int. Conf. Med. Image Comput. Comput.-Assist. Interv., Springer, 2016: pp. 229–237. http://link.springer.com/chapter/10.1007/978-3-319-46726-9_27 (accessed July 24, 2017).
[132] J. Zhang, M. Liu, D. Shen, Detecting Anatomical Landmarks From Limited Medical Imaging Data Using Two-Stage Task-Oriented Deep Neural Networks, IEEE Trans. Image Process. Publ. IEEE Signal Process. Soc. 26 (2017) 4753–4764. doi:10.1109/TIP.2017.2721106.
[133] A. Esteva, B. Kuprel, R.A. Novoa, J. Ko, S.M. Swetter, H.M. Blau, S. Thrun, Dermatologist-level classification of skin cancer with deep neural networks, Nature. 542 (2017) 115–118. doi:10.1038/nature21056.
[134] K.-L. Hua, C.-H. Hsu, S.C. Hidayati, W.-H. Cheng, Y.-J. Chen, Computer-aided classification of lung nodules on computed tomography images via deep learning technique, OncoTargets Ther. 8 (2015) 2015–2022. doi:10.2147/OTT.S80733.
[135] D. Kumar, A. Wong, D.A. Clausi, Lung nodule classification using deep features in CT images, in: Comput. Robot Vis. CRV 2015 12th Conf. On, IEEE, 2015: pp. 133–138. http://ieeexplore.ieee.org/abstract/document/7158331/ (accessed February 6, 2017).
[136] Q. Song, L. Zhao, X. Luo, X. Dou, Using Deep Learning for Classification of Lung Nodules on Computed Tomography Images, J. Healthc. Eng. 2017 (2017). doi:10.1155/2017/8314740.
[137] W. Sun, B. Zheng, W. Qian, Automatic feature learning using multichannel ROI based on deep structured algorithms for computerized lung cancer diagnosis, Comput. Biol. Med. 89 (2017) 530–539. doi:10.1016/j.compbiomed.2017.04.006.
[138] H. Wang, Z. Zhou, Y. Li, Z. Chen, P. Lu, W. Wang, W. Liu, L. Yu, Comparison of machine learning methods for classifying mediastinal lymph node metastasis of non-small cell lung cancer from 18 F-FDG PET/CT images, EJNMMI Res. 7 (2017) 11. doi:10.1186/s13550-017-0260-9.
[139] T. Kooi, B. van Ginneken, N. Karssemeijer, A. den Heeten, Discriminating solitary cysts from soft tissue lesions in mammography using a pretrained deep convolutional neural network, Med. Phys. 44 (2017) 1017–1027. doi:10.1002/mp.12110.
[140] A. Akselrod-Ballin, L. Karlinsky, S. Alpert, S. Hasoul, R. Ben-Ari, E. Barkan, A Region Based Convolutional Network for Tumor Detection and Classification in Breast Mammography, in:

Deep Learn. Data Labeling Med. Appl., Springer, Cham, 2016: pp. 197–205. doi:10.1007/978-3-319-46976-8_21.

[141] Q. Chen, X. Xu, S. Hu, X. Li, Q. Zou, Y. Li, A transfer learning approach for classification of clinical significant prostate cancers from mpMRI scans, in: 2017: p. 101344F–101344F–4. doi:10.1117/12.2279021.

[142] I. Banerjee, A. Crawley, M. Bhethanabotla, H.E. Daldrup-Link, D.L. Rubin, Transfer learning on fused multiparametric MR images for classifying histopathological subtypes of rhabdomyosarcoma, Comput. Med. Imaging Graph. Off. J. Comput. Med. Imaging Soc. (2017). doi:10.1016/j.compmedimag.2017.05.002.

[143] X. Yang, R. Kwitt, M. Niethammer, Fast Predictive Image Registration, in: Deep Learn. Data Labeling Med. Appl., Springer, Cham, 2016: pp. 48–57. doi:10.1007/978-3-319-46976-8_6.

[144] S. Miao, Z.J. Wang, Y. Zheng, R. Liao, Real-time 2D/3D registration via CNN regression, in: Biomed. Imaging ISBI 2016 IEEE 13th Int. Symp. On, IEEE, 2016: pp. 1430–1434. http://ieeexplore.ieee.org/abstract/document/7493536/ (accessed February 15, 2017).

[145] B. Hou, A. Alansary, S. McDonagh, A. Davidson, M. Rutherford, J.V. Hajnal, D. Rueckert, B. Glocker, B. Kainz, Predicting Slice-to-Volume Transformation in Presence of Arbitrary Subject Motion, ArXiv170208891 Cs. (2017). http://arxiv.org/abs/1702.08891 (accessed March 29, 2017).

[146] G. Wu, M. Kim, Q. Wang, B.C. Munsell, D. Shen, Scalable High-Performance Image Registration Framework by Unsupervised Deep Feature Representations Learning, IEEE Trans. Biomed. Eng. 63 (2016) 1505–1516. doi:10.1109/TBME.2015.2496253.

[147] K. Ma, J. Wang, V. Singh, B. Tamersoy, Y.-J. Chang, A. Wimmer, T. Chen, Multimodal Image Registration with Deep Context Reinforcement Learning, in: Med. Image Comput. Comput. Assist. Interv. − MICCAI 2017, Springer, Cham, 2017: pp. 240–248. doi:10.1007/978-3-319-66182-7_28.

[148] S. Miao, S. Piat, P. Fischer, A. Tuysuzoglu, P. Mewes, T. Mansi, R. Liao, Dilated FCN for Multi-Agent 2D/3D Medical Image Registration, ArXiv171201651 Cs. (2017). http://arxiv.org/abs/1712.01651.

[149] D. Nguyen, T. Long, X. Jia, W. Lu, X. Gu, Z. Iqbal, S. Jiang, Dose Prediction with U-net: A Feasibility Study for Predicting Dose Distributions from Contours using Deep Learning on Prostate IMRT Patients, ArXiv Prepr. ArXiv170909233. (2017).

[150] M. Mardani, P. Dong, L. Xing, Deep-Learning Based Prediction of Achievable Dose for Personalizing Inverse Treatment Planning, Int. J. Radiat. Oncol. 96 (2016) E419–E420. doi:http://dx.doi.org/10.1016/j.ijrobp.2016.06.1685.

[151] M. Mardani Korani, P. Dong, L. Xing, MO-G-201-03: Deep-Learning Based Prediction of Achievable Dose for Personalizing Inverse Treatment Planning, Med. Phys. 43 (2016) 3724. doi:10.1118/1.4957369.

[152] O. Ogunmolu, X. Gu, S. Jiang, N. Gans, Nonlinear Systems Identification Using Deep Dynamic Neural Networks, ArXiv Prepr. ArXiv161001439. (2016). https://arxiv.org/abs/1610.01439 (accessed February 15, 2017).

[153] T. Terunuma, A. Tokui, T. Sakae, Novel real-time tumor-contouring method using deep learning to prevent mistracking in X-ray fluoroscopy, Radiol. Phys. Technol. (2017) 1–11. doi:10.1007/s12194-017-0435-0.

[154] Park, Intra- and Inter-Fractional Variation Prediction of Lung Tumors Using Fuzzy Deep Learning, IEEE J. Transl. Eng. Health Med. 4 (2016). doi:10.1109/JTEHM.2016.2516005.

[155] A. Santhanam, Y. Min, P. Beron, N. Agazaryan, P. Kupelian, D. Low, SU-D-201-05: On the Automatic Recognition of Patient Safety Hazards in a Radiotherapy Setup Using a Novel 3D Camera System and a Deep Learning Framework, Med. Phys. 43 (2016) 3334–3335. doi:10.1118/1.4955617.

[156] S. Aneja, U. Shaham, R.J. Kumar, N. Pirakitikulr, S.K. Nath, J.B. Yu, D.J. Carlson, R.H. Decker, Deep Neural Network to Predict Local Failure Following Stereotactic Body Radiation Therapy:

Integrating Imaging and Clinical Data to Predict Outcomes, Int J Radiat Oncol Biol. 99 (2017) S47. doi:10.1016/j.ijrobp.2017.06.120.

[157] H. Li, H. Zhong, P.J. Boimel, E. Ben-Josef, Y. Xiao, Y. Fan, Deep Convolutional Neural Networks for Imaging Based Survival Analysis of Rectal Cancer Patients, Int J Radiat Oncol Biol. 99 (2017) S183. doi:10.1016/j.ijrobp.2017.06.458.

[158] X. Qi, J. Neylon, A. Santhanam, Dosimetric Predictors for Quality of Life After Prostate Stereotactic Body Radiation Therapy via Deep Learning Network, Int J Radiat Oncol Biol. 99 (2017) S167. doi:10.1016/j.ijrobp.2017.06.384.

[159] X. Zhen, J. Chen, Z. Zhong, B.A. Hrycushko, K. Albuquerque, L. Zhou, S.B. Jiang, X. Gu, Deep Convolutional Neural Networks With Transfer Learning for Rectum Toxicity Prediction in Combined Brachytherapy and External Beam Radiation Therapy for Cervical Cancer, Int J Radiat Oncol Biol. 99 (2017) S168. doi:10.1016/j.ijrobp.2017.06.386.

[160] A. Jochems, T.M. Deist, I. El Naqa, M. Kessler, C. Mayo, J. Reeves, S. Jolly, M. Matuszak, R. Ten Haken, J. van Soest, C. Oberije, C. Faivre-Finn, G. Price, D. de Ruysscher, P. Lambin, A. Dekker, Developing and Validating a Survival Prediction Model for NSCLC Patients Through Distributed Learning Across 3 Countries, Int. J. Radiat. Oncol. 99 (2017) 344–352. doi:10.1016/j.ijrobp.2017.04.021.

[161] H.-H. Tseng, Y. Luo, S. Cui, J.-T. Chien, R.K. Ten Haken, I.E. Naqa, Deep reinforcement learning for automated radiation adaptation in lung cancer, Med. Phys. 44 (2017) 6690–6705. doi:10.1002/mp.12625.

[162] A. Qayyum, S.M. Anwar, M. Awais, M. Majid, Medical image retrieval using deep convolutional neural network, Neurocomputing. 266 (2017) 8–20. doi:10.1016/j.neucom.2017.05.025.

[163] Y. Wu, M. Jiang, J. Lei, H. Xu, Named Entity Recognition in Chinese Clinical Text Using Deep Neural Network, Stud. Health Technol. Inform. 216 (2015) 624–628.

[164] X. Lv, Y. Guan, J. Yang, J. Wu, Clinical Relation Extraction with Deep Learning, Int. J. Hybrid Inf. Technol. 9 (2016) 237–248. doi:10.14257/ijhit.2016.9.7.22.

[165] J.M. Edmund, T. Nyholm, A review of substitute CT generation for MRI-only radiation therapy, Radiat. Oncol. Lond. Engl. 12 (2017) 28. doi:10.1186/s13014-016-0747-y.

[166] E. Persson, C. Gustafsson, F. Nordström, M. Sohlin, A. Gunnlaugsson, K. Petruson, N. Rintelä, K. Hed, L. Blomqvist, B. Zackrisson, T. Nyholm, L.E. Olsson, C. Siversson, J. Jonsson, MR-OPERA: A Multicenter/Multivendor Validation of Magnetic Resonance Imaging–Only Prostate Treatment Planning Using Synthetic Computed Tomography Images, Int. J. Radiat. Oncol. 99 (2017) 692–700. doi:10.1016/j.ijrobp.2017.06.006.

[167] M.L. Nguyen, B. Willows, R. Khan, A. Chi, L. Kim, S.G. Nour, T. Sroka, C. Kerr, J. Godinez, M. Mills, U. Karlsson, G. Altdorfer, N.P. Nguyen, G. Jendrasiak, The Potential Role of Magnetic Resonance Spectroscopy in Image-Guided Radiotherapy, Front. Oncol. 4 (2014). doi:10.3389/fonc.2014.00091.

[168] D. Giantsoudi, B. De Man, J. Verburg, A. Trofimov, Y. Jin, G. Wang, L. Gjesteby, H. Paganetti, Metal artifacts in computed tomography for radiation therapy planning: dosimetric effects and impact of metal artifact reduction, Phys. Med. Biol. 62 (2017) R49–R80. doi:10.1088/1361-6560/aa5293.

[169] D.G. Kovacs, L.A. Rechner, A.L. Appelt, A.K. Berthelsen, J.C. Costa, J. Friborg, G.F. Persson, J.P. Bangsgaard, L. Specht, M.C. Aznar, Metal artefact reduction for accurate tumour delineation in radiotherapy, Radiother. Oncol. 126 (2018) 479–486. doi:10.1016/j.radonc.2017.09.029.

[170] D.C. Alexander, D. Zikic, A. Ghosh, R. Tanno, V. Wottschel, J. Zhang, E. Kaden, T.B. Dyrby, S.N. Sotiropoulos, H. Zhang, A. Criminisi, Image quality transfer and applications in diffusion MRI, NeuroImage. 152 (2017) 283–298. doi:10.1016/j.neuroimage.2017.02.089.

[171] G.T.Y. Chen, G.C. Sharp, S. Mori, A review of image-guided radiotherapy, Radiol. Phys. Technol. 2 (2009) 1–12. doi:10.1007/s12194-008-0045-y.

[172] S.G. Tejinder Kataria, Image Guided Radiation Therapy, J. Nucl. Med. Radiat. Ther. 05 (2014). doi:10.4172/2155-9619.1000179.
[173] D.A. Jaffray, Image-guided radiotherapy: from current concept to future perspectives, Nat. Rev. Clin. Oncol. 9 (2012) 688–699. doi:10.1038/nrclinonc.2012.194.
[174] I. Arivarasan, C. Anuradha, S. Subramanian, A. Anantharaman, V. Ramasubramanian, Magnetic resonance image guidance in external beam radiation therapy planning and delivery, Jpn. J. Radiol. 35 (2017) 417–426. doi:10.1007/s11604-017-0656-5.
[175] J. Simon, F. Eschwege, L.E. Hajj, V. Marchesi, A. Noel, M. Levitchi, C. Marchal, P. Gourmelon, D. Peiffert, Epinal #2: 409 Patients Overexposed during Radiotherapy for Prostate Cancer after Daily Use of Portal Imaging Controls, Int. J. Radiat. Oncol. • Biol. • Phys. 78 (2010) S361. doi:10.1016/j.ijrobp.2010.07.852.
[176] D.L. Pham, C. Xu, J.L. Prince, Current methods in medical image segmentation, Annu. Rev. Biomed. Eng. 2 (2000) 315–337. doi:10.1146/annurev.bioeng.2.1.315.
[177] D. Whitey, Z. Koles, A review of medial image segmentation, Int. J. Bioelectromagn. 10 (2008) 125–148.
[178] Z. Akkus, A. Galimzianova, A. Hoogi, D.L. Rubin, B.J. Erickson, Deep Learning for Brain MRI Segmentation: State of the Art and Future Directions, J. Digit. Imaging. 30 (2017) 449–459. doi:10.1007/s10278-017-9983-4.
[179] B.H. Menze, A. Jakab, S. Bauer, J. Kalpathy-Cramer, K. Farahani, J. Kirby, Y. Burren, N. Porz, J. Slotboom, R. Wiest, L. Lanczi, E. Gerstner, M.A. Weber, T. Arbel, B.B. Avants, N. Ayache, P. Buendia, D.L. Collins, N. Cordier, J.J. Corso, A. Criminisi, T. Das, H. Delingette, ??a??atay Demiralp, C.R. Durst, M. Dojat, S. Doyle, J. Festa, F. Forbes, E. Geremia, B. Glocker, P. Golland, X. Guo, A. Hamamci, K.M. Iftekharuddin, R. Jena, N.M. John, E. Konukoglu, D. Lashkari, J.A. Mariz, R. Meier, S. Pereira, D. Precup, S.J. Price, T.R. Raviv, S.M.S. Reza, M. Ryan, D. Sarikaya, L. Schwartz, H.C. Shin, J. Shotton, C.A. Silva, N. Sousa, N.K. Subbanna, G. Szekely, T.J. Taylor, O.M. Thomas, N.J. Tustison, G. Unal, F. Vasseur, M. Wintermark, D.H. Ye, L. Zhao, B. Zhao, D. Zikic, M. Prastawa, M. Reyes, K. Van Leemput, The Multimodal Brain Tumor Image Segmentation Benchmark (BRATS), IEEE Trans. Med. Imaging. 34 (2015) 1993–2024. doi:10.1109/TMI.2014.2377694.
[180] MICCAI BRATS - The Multimodal Brain Tumor Segmentation Challenge, (n.d.). http://braintumorsegmentation.org/ (accessed September 27, 2017).
[181] A. Işın, C. Direkoğlu, M. Şah, Review of MRI-based Brain Tumor Image Segmentation Using Deep Learning Methods, Procedia Comput. Sci. 102 (2016) 317–324. doi:http://dx.doi.org/10.1016/j.procs.2016.09.407.
[182] M. Shahedi, D.W. Cool, G.S. Bauman, M. Bastian-Jordan, A. Fenster, A.D. Ward, Accuracy Validation of an Automated Method for Prostate Segmentation in Magnetic Resonance Imaging, J. Digit. Imaging. (2017). doi:10.1007/s10278-017-9964-7.
[183] J. Ferlay, I. Soerjomataram, R. Dikshit, S. Eser, C. Mathers, M. Rebelo, D.M. Parkin, D. Forman, F. Bray, Cancer incidence and mortality worldwide: sources, methods and major patterns in GLOBOCAN 2012, Int. J. Cancer. 136 (2015) E359-386. doi:10.1002/ijc.29210.
[184] A. Mehrtash, M. Pesteie, J. Hetherington, P.A. Behringer, T. Kapur, W.M. Wells, R. Rohling, A. Fedorov, P. Abolmaesumi, DeepInfer: Open-Source Deep Learning Deployment Toolkit for Image-Guided Therapy, Proc. SPIE-- Int. Soc. Opt. Eng. 10135 (2017). doi:10.1117/12.2256011.
[185] C. Chu, J. De Fauw, N. Tomasev, B.R. Paredes, C. Hughes, J. Ledsam, T. Back, H. Montgomery, G. Rees, R. Raine, others, Applying machine learning to automated segmentation of head and neck tumour volumes and organs at risk on radiotherapy planning CT and MRI scans, F1000Research. 5 (2016). https://f1000research.com/articles/5-2104/v1 (accessed January 16, 2017).
[186] Y. Yuan, M. Chao, Y.C. Lo, Automatic Skin Lesion Segmentation Using Deep Fully Convolutional Networks with Jaccard Distance, IEEE Trans. Med. Imaging. PP (2017) 1–1. doi:10.1109/TMI.2017.2695227.

[187] Y. Yuan, Y.C. Lo, Improving Dermoscopic Image Segmentation with Enhanced Convolutional-Deconvolutional Networks, IEEE J. Biomed. Health Inform. PP (2017) 1–1. doi:10.1109/JBHI.2017.2787487.
[188] D. Fontanarosa, S. van der Meer, J. Bamber, E. Harris, T. O'Shea, F. Verhaegen, Review of ultrasound image guidance in external beam radiotherapy: I. Treatment planning and inter-fraction motion management, Phys. Med. Biol. 60 (2015) R77. doi:10.1088/0031-9155/60/3/R77.
[189] T. O'Shea, J. Bamber, D. Fontanarosa, S. van der Meer, F. Verhaegen, E. Harris, Review of ultrasound image guidance in external beam radiotherapy part II: intra-fraction motion management and novel applications, Phys. Med. Biol. 61 (2016) R90. doi:10.1088/0031-9155/61/8/R90.
[190] S.A. Mason, T.P. O'Shea, I.M. White, S. Lalondrelle, K. Downey, M. Baker, C.F. Behrens, J.C. Bamber, E.J. Harris, Towards ultrasound-guided adaptive radiotherapy for cervical cancer: Evaluation of Elekta's semiautomated uterine segmentation method on 3D ultrasound images, Med. Phys. 44 (2017) 3630–3638. doi:10.1002/mp.12325.
[191] S. Nouranian, M. Ramezani, I. Spadinger, W.J. Morris, S.E. Salcudean, P. Abolmaesumi, Learning-Based Multi-Label Segmentation of Transrectal Ultrasound Images for Prostate Brachytherapy, IEEE Trans. Med. Imaging. 35 (2016) 921–932. doi:10.1109/TMI.2015.2502540.
[192] K. Doi, Computer-Aided Diagnosis in Medical Imaging: Historical Review, Current Status and Future Potential, Comput. Med. Imaging Graph. Off. J. Comput. Med. Imaging Soc. 31 (2007) 198–211. doi:10.1016/j.compmedimag.2007.02.002.
[193] I.R.S. Valente, P.C. Cortez, E.C. Neto, J.M. Soares, V.H.C. de Albuquerque, J.M.R. Tavares, Automatic 3D pulmonary nodule detection in CT images: a survey, Comput. Methods Programs Biomed. 124 (2016) 91–107.
[194] V.J. Mar, R.A. Scolyer, G.V. Long, Computer-assisted diagnosis for skin cancer: have we been outsmarted?, Lancet Lond. Engl. 389 (2017) 1962–1964. doi:10.1016/S0140-6736(17)31285-0.
[195] S.G. Armato, K. Drukker, F. Li, L. Hadjiiski, G.D. Tourassi, R.M. Engelmann, M.L. Giger, G. Redmond, K. Farahani, J.S. Kirby, L.P. Clarke, LUNGx Challenge for computerized lung nodule classification, J. Med. Imaging. 3 (2016) 044506. doi:10.1117/1.JMI.3.4.044506.
[196] L. Sunwoo, Y.J. Kim, S.H. Choi, K.-G. Kim, J.H. Kang, Y. Kang, Y.J. Bae, R.-E. Yoo, J. Kim, K.J. Lee, others, Computer-aided detection of brain metastasis on 3D MR imaging: Observer performance study, PloS One. 12 (2017) e0178265.
[197] S. Belharbi, C. Chatelain, R. Hérault, S. Adam, S. Thureau, M. Chastan, R. Modzelewski, Spotting L3 slice in CT scans using deep convolutional network and transfer learning, Comput. Biol. Med. (2017). doi:10.1016/j.compbiomed.2017.05.018.
[198] K.K. Brock, S. Mutic, T.R. McNutt, H. Li, M.L. Kessler, Use of image registration and fusion algorithms and techniques in radiotherapy: Report of the AAPM Radiation Therapy Committee Task Group No. 132, Med. Phys. 44 (2017) e43–e76. doi:10.1002/mp.12256.
[199] M.A. Viergever, J.B.A. Maintz, S. Klein, K. Murphy, M. Staring, J.P.W. Pluim, A survey of medical image registration – under review, Med. Image Anal. 33 (2016) 140–144. doi:10.1016/j.media.2016.06.030.
[200] S. Wang, D. Zheng, C. Zhang, R. Ma, N.R. Bennion, Y. Lei, X. Zhu, C.A. Enke, S. Zhou, Automatic planning on hippocampal avoidance whole-brain radiotherapy, Med. Dosim. 42 (2017) 63–68. doi:10.1016/j.meddos.2016.12.002.
[201] K. Nawa, A. Haga, A. Nomoto, R.A. Sarmiento, K. Shiraishi, H. Yamashita, K. Nakagawa, Evaluation of a commercial automatic treatment planning system for prostate cancers, Med. Dosim. 42 (2017) 203–209. doi:10.1016/j.meddos.2017.03.004.
[202] C. Schubert, O. Waletzko, C. Weiss, D. Voelzke, S. Toperim, A. Roeser, S. Puccini, M. Piroth, C. Mehrens, J.-D. Kueter, K. Hierholz, K. Gerull, A. Fogliata, A. Block, L. Cozzi, Intercenter validation of a knowledge based model for automated planning of volumetric modulated arc

therapy for prostate cancer. The experience of the German RapidPlan Consortium, PLOS ONE. 12 (2017) e0178034. doi:10.1371/journal.pone.0178034.

[203] R.A. Mitchell, P. Wai, R. Colgan, A.M. Kirby, E.M. Donovan, Improving the efficiency of breast radiotherapy treatment planning using a semi-automated approach, J. Appl. Clin. Med. Phys. 18 (2017) 18–24. doi:10.1002/acm2.12006.

[204] C. McIntosh, M. Welch, A. McNiven, D.A. Jaffray, T.G. Purdie, Fully automated treatment planning for head and neck radiotherapy using a voxel-based dose prediction and dose mimicking method, Phys. Med. Biol. 62 (2017) 5926–5944. doi:10.1088/1361-6560/aa71f8.

[205] J. Fan, J. Wang, Z. Zhang, W. Hu, Iterative dataset optimization in automated planning: Implementation for breast and rectal cancer radiotherapy, Med. Phys. 44 (2017) 2515–2531. doi:10.1002/mp.12232.

[206] J.J. Boutilier, T. Craig, M.B. Sharpe, T.C.Y. Chan, Sample size requirements for knowledge-based treatment planning, Med. Phys. 43 (2016) 1212–1221. doi:10.1118/1.4941363.

[207] H. Wang, P. Dong, H. Liu, L. Xing, Development of an autonomous treatment planning strategy for radiation therapy with effective use of population-based prior data, Med. Phys. 44 (2017) 389–396. doi:10.1002/mp.12058.

[208] D. Yan, F. Vicini, J. Wong, A. Martinez, Adaptive radiation therapy, Phys. Med. Biol. 42 (1997) 123–132.

[209] A.J. McPartlin, X.A. Li, L.E. Kershaw, U. Heide, L. Kerkmeijer, C. Lawton, U. Mahmood, F. Pos, N. van As, M. van Herk, D. Vesprini, J. van der Voort van Zyp, A. Tree, A. Choudhury, MRI-guided prostate adaptive radiotherapy – A systematic review, Radiother. Oncol. 119 (2016) 371–380. doi:10.1016/j.radonc.2016.04.014.

[210] E. Colvill, J. Booth, S. Nill, M. Fast, J. Bedford, U. Oelfke, M. Nakamura, P. Poulsen, E. Worm, R. Hansen, T. Ravkilde, J. Scherman Rydh?g, T. Pommer, P. Munck af Rosenschold, S. Lang, M. Guckenberger, C. Groh, C. Herrmann, D. Verellen, K. Poels, L. Wang, M. Hadsell, T. Sothmann, O. Blanck, P. Keall, A dosimetric comparison of real-time adaptive and non-adaptive radiotherapy: A multi-institutional study encompassing robotic, gimbaled, multileaf collimator and couch tracking, Radiother. Oncol. 119 (2016) 159–165. doi:10.1016/j.radonc.2016.03.006.

[211] S. Lim-Reinders, B.M. Keller, S. Al-Ward, A. Sahgal, A. Kim, Online Adaptive Radiation Therapy, Int. J. Radiat. Oncol. 99 (2017) 994–1003. doi:10.1016/j.ijrobp.2017.04.023.

[212] L.P. Muren, N. Jornet, D. Georg, R. Garcia, D.I. Thwaites, Improving radiotherapy through medical physics developments, Radiother. Oncol. 117 (2015) 403–406. doi:10.1016/j.radonc.2015.11.008.

[213] D.T. Nguyen, R. O'Brien, J.-H. Kim, C.-Y. Huang, L. Wilton, P. Greer, K. Legge, J.T. Booth, P.R. Poulsen, J. Martin, P.J. Keall, The first clinical implementation of a real-time six degree of freedom target tracking system during radiation therapy based on Kilovoltage Intrafraction Monitoring (KIM), Radiother. Oncol. 123 (2017) 37–42. doi:10.1016/j.radonc.2017.02.013.

[214] M. Glitzner, M.F. Fast, B.D. de Senneville, S. Nill, U. Oelfke, J.J.W. Lagendijk, B.W. Raaymakers, S.P.M. Crijns, Real-time auto-adaptive margin generation for MLC-tracked radiotherapy, Phys. Med. Biol. 62 (2017) 186–201. doi:10.1088/1361-6560/62/1/186.

[215] T. Lin, Y. Lin, Markerless Tumor Gating and Tracking for Lung Cancer Radiotherapy based on Machine Learning Techniques, in: Artif. Intell. Decis. Support Syst. Diagn. Med. Imaging, Springer, Cham, 2018: pp. 337–359. doi:10.1007/978-3-319-68843-5_12.

[216] O.P. Ogunmolu, X. Gu, S. Jiang, N.R. Gans, A real-time, soft robotic patient positioning system for maskless head-and-neck cancer radiotherapy: An initial investigation, in: 2015 IEEE Int. Conf. Autom. Sci. Eng. CASE, 2015: pp. 1539–1545. doi:10.1109/CoASE.2015.7294318.

[217] O.P. Ogunmolu, X. Gu, S. Jiang, N.R. Gans, Vision-based control of a soft robot for maskless head and neck cancer radiotherapy, in: 2016 IEEE Int. Conf. Autom. Sci. Eng. CASE, 2016: pp. 180–187. doi:10.1109/COASE.2016.7743378.

[218] M. Schwarz, G.M. Cattaneo, L. Marrazzo, Geometrical and dosimetrical uncertainties in hypofractionated radiotherapy of the lung: A review, Phys. Med. 36 (2017) 126–139. doi:10.1016/j.ejmp.2017.02.011.
[219] J.-E. Bibault, P. Giraud, A. Burgun, Big Data and machine learning in radiation oncology: State of the art and future prospects, Cancer Lett. 382 (2016) 110–117. doi:10.1016/j.canlet.2016.05.033.
[220] O. Ylijoki, J. Porras, Perspectives to definition of big data: a mapping study and discussion, J. Innov. Manag. 4 (2016) 69–91.
[221] G.S. Birkhead, M. Klompas, N.R. Shah, Uses of Electronic Health Records for Public Health Surveillance to Advance Public Health, Annu. Rev. Public Health. 36 (2015) 345–359. doi:10.1146/annurev-publhealth-031914-122747.
[222] Ö. Uzuner, B.R. South, S. Shen, S.L. DuVall, 2010 i2b2/VA challenge on concepts, assertions, and relations in clinical text, J. Am. Med. Inform. Assoc. JAMIA. 18 (2011) 552–556. doi:10.1136/amiajnl-2011-000203.
[223] J. Kang, R. Schwartz, J. Flickinger, S. Beriwal, Machine Learning Approaches for Predicting Radiation Therapy Outcomes: A Clinician's Perspective, Int J Radiat Oncol Biol. 93 (2015) 1127–1135. doi:http://dx.doi.org/10.1016/j.ijrobp.2015.07.2286.
[224] S. Lee, K.H. Kim, C.S. Woo, J.B. Shim, Y.J. Cao, K.H. Chang, C.Y. Kim, Predictive Solution for Radiation Toxicity Based on Big Data, in: Radiotherapy, InTech, 2017. https://www.intechopen.com/books/radiotherapy/predictive-solution-for-radiation-toxicity-based-on-big-data (accessed May 24, 2017).
[225] C.M. Lynch, V.H. van Berkel, H.B. Frieboes, Application of unsupervised analysis techniques to lung cancer patient data, PLOS ONE. 12 (2017) e0184370.
[226] S.K. Das, S. Zhou, J. Zhang, F.-F. Yin, M.W. Dewhirst, L.B. Marks, Predicting Lung Radiotherapy-Induced Pneumonitis Using a Model Combining Parametric Lyman Probit Withnonparametric Decision Trees, Int J Radiat Oncol Biol. 68 (2007) 1212–1221. doi:10.1016/j.ijrobp.2007.03.064.
[227] G. Cosma, D. Brown, M. Archer, M. Khan, A.G. Pockley, A survey on computational intelligence approaches for predictive modeling in prostate cancer, Expert Syst. Appl. 70 (2017) 1–19. doi:http://dx.doi.org/10.1016/j.eswa.2016.11.006.
[228] J.A. Dean, K.H. Wong, L.C. Welsh, A.-B. Jones, U. Schick, K.L. Newbold, S.A. Bhide, K.J. Harrington, C.M. Nutting, S.L. Gulliford, Normal tissue complication probability (NTCP) modelling using spatial dose metrics and machine learning methods for severe acute oral mucositis resulting from head and neck radiotherapy, Radiother. Oncol. J. Eur. Soc. Ther. Radiol. Oncol. 120 (2016) 21–27. doi:10.1016/j.radonc.2016.05.015.
[229] J. Coates, L. Souhami, I. El Naqa, Big Data Analytics for Prostate Radiotherapy, Front. Oncol. 6 (2016). doi:10.3389/fonc.2016.00149.
[230] B. Salazar, E. Balczewski, C. Ung, S. Zhu, Neuroblastoma, a Paradigm for Big Data Science in Pediatric Oncology, Int. J. Mol. Sci. 18 (2016) 37. doi:10.3390/ijms18010037.
[231] R.S. Muthalaly, Using Deep Learning to predict the mortality of Leukemia patients, Queen's University (Kingston, Ont.), 2017. http://qspace.library.queensu.ca/handle/1974/15929 (accessed July 12, 2017).
[232] A. Nguyen, J. Yosinski, J. Clune, Deep neural networks are easily fooled: High confidence predictions for unrecognizable images, in: Proc. IEEE Conf. Comput. Vis. Pattern Recognit., 2015: pp. 427–436.
[233] M. Havaei, N. Guizard, H. Larochelle, P.-M. Jodoin, Deep Learning Trends for Focal Brain Pathology Segmentation in MRI, in: Mach. Learn. Health Inform., Springer, Cham, 2016: pp. 125–148. doi:10.1007/978-3-319-50478-0_6.
[234] S.H. Benedict, K. Hoffman, M.K. Martel, A.P. Abernethy, A.L. Asher, J. Capala, R.C. Chen, B. Chera, J. Couch, J. Deye, J.A. Efstathiou, E. Ford, B.A. Fraass, P.E. Gabriel, V. Huser, B.D. Kavanagh, D. Khuntia, L.B. Marks, C. Mayo, T. McNutt, R.S. Miller, K.L. Moore, F. Prior, E.

Roelofs, B.S. Rosenstein, J. Sloan, A. Theriault, B. Vikram, Overview of the American Society for Radiation Oncology–National Institutes of Health–American Association of Physicists in Medicine Workshop 2015: Exploring Opportunities for Radiation Oncology in the Era of Big Data, Int J Radiat Oncol Biol. 95 (2016) 873–879. doi:10.1016/j.ijrobp.2016.03.006.

- a review of deep learning methods applied to radiotherapy is proposed
- a deep-learning explanation intended for the radiotherapy community is presented
- reviewed papers are classified into seven categories related to the patient workflow